REVIEWS OF

MODERN PHYSICS

VOLUME 41, NUMBER 2 APRIL 1969

Low-Energy Electron-Diffraction Dispersion Surfaces and Band Structure in Three-Dimensional Mixed Laue and Bragg Reflections*

R. M. STERN, J. J. PERRY, D. S. BOUDREAUX

Department of Physics, Polytechnic Institute of Brooklyn, Brooklyn, New York

Although the theory of the propagation of electron waves in periodic solids and the theory of the elastic diffraction of electron waves by periodic solids have developed independently into band theory and dynamical electron-diffraction theory, respectively, they are in fact formally identical. The electron wave functions which can exist in the crystal are determined by a seven-dimensional hypersurface in energy-complex **K** space which defines the totality of solutions to the wave equation in the infinite crystal. In the diffraction problem, the introduction of the crystal surface together with the magnitude and direction of the external electron wave vector selects the particular set of eigenfunctions which are excited during a given experiment and which correspond to the allowed electron states in the crystal. This set constitutes the wave field in the self-consistent multiple-scattering approach. It is demonstrated that the energy band diagram of band theory and the constant energy dispersion surface of dynamical theory are in fact sections of the same hypersurface. The complex nature of the dispersion surface leads to the excitation of evanescent waves both in the crystal and in the vacuum. The diffraction boundary conditions, notably conservation of total energy and of momentum parallel to the crystal surface, can easily be introduced, geometrically, by means of a constraint surface which contains the crystal normal. In a given experiment the excited wave functions are determined by the intersection of the hypersurface with the appropriate constraint surface. It is shown that the most useful constraint surfaces are those at constant energy and furthermore that the dispersion hypersurface is an ameniable method for the discussion of low-energy electron-diffraction (LEED) cases of high order and high symmetry, several of which are outlined in detail. The variation of the reflected intensities observed in electron-diffraction experiments is discussed in terms of the changes in the allowed electron wave functions as calculated by three-dimensional band-structure and/or dynamical diffraction theory. In particular, we predict zeros in the reflected Bragg intensities for certain special geometries in the case of two simultaneous reflections (mixed Bragg–Laue case).

CONTENTS

I. INTRODUCTION

Measurements of intensity in low energy electron diffraction (LEED) as a function of the diffraction parameters are characterized by extensive fine structure. Because of the appearance of maxima in the intensity which violate strict three-dimensional crystal symmetry and because of the expected large magnitude of the atomic scattering cross sections in the energy range studied (10–1000 eV), analysis of LEED observations has emphasized the two-dimensional aspects of the problem. Electron-diffraction theories (Bethe, 1928; McRae, 1966; Kambe, 1967; Plaskett, 1967; Boudreaux and Heine, 1967; Tournarie, 1962; Marcus and Jepsen, 1968) have been developed which can in principle be made exact. Those most applicable at low energies have emphasized the heretofore unexplained surface-related effects; e.g., non-Bragg frac-

* Supported in part by USAFOSR Grant 1263–67.

tional order peaks and surface wave resonances. However, the utilization of techniques common to high-energy electron diffraction and to x-ray diffraction, where the intensity is studied as a function of three-dimensional diffraction parameters,* has indicated that the diffracting crystal is indeed three dimensional. Recent measurements in this laboratory indicate that the inclusion of the effects of simultaneous reflections (multiple diffraction) in a three-dimensional model successfully accounts for the geometrical origin of most of the fine structure observed (Gervais, Stern, and Menes, 1968; Taub and Stern, 1968; Stern and Taub, 1968; Gervais and Stern, 1968; Stern, Taub, and Gervais, 1968; Stern, 1968).

The understanding of the origin of the intensity variation with diffraction parameters in LEED measurements therefore requires the development of a three-dimensional dynamical diffraction theory or its equivalent. The purpose of this article is not to review existing theories in detail but to show, in particular, the mathematical formalism, and hence the underlying physics, of the band-structure approach (Boudreaux and Heine, 1967) and the dynamical diffraction theory of Bethe (1928) for electrons in triperiodic media are identical. We will demonstrate that the energy-band diagram of band theory and the (constant-energy) dispersion surface of dynamical theory† are in fact sections of the same seven-dimensional dispersion hypersurface in energy-complex $\mathbf{K}$ space $(E, \mathbf{K}^r, \mathbf{K}^i)$, which defines the totality of allowed electronic states in the crystal.‡

The introduction of the idealized crystal surface (which leaves the semi-infinite crystal intact) does no more than introduce boundary conditions. The constraints imposed by the satisfaction of the boundary conditions in any diffraction experiment determine a particular constraint surface in this hyperspace which contains all the solutions allowed by the boundary conditions. The intersection of this constraint surface and the dispersion hypersurface selects the eigenfunctions excited in the crystal by that experiment. In particular, to prevent divergences in the electronic density from developing, the only imaginary components of $\mathbf{K}$ which are allowed to exist are those normal to the crystal surfaces.

The eigenfunctions of real $\mathbf{K}$ contain the traveling waves of the problem; however, it is the relative amplitudes of all the eigenfunctions of real and complex $\mathbf{K}$ which determine the diffracted intensities. The latter part of this paper will be concerned with a discussion indicating how a qualitative determination of the relative plane-wave amplitudes can be made on the basis of simple approximations for certain symmetrical cases. In particular, for the case where two reflections which lie in the plane of incidence are simultaneously excited, the real two-dimensional dispersion surface will be shown. A description will be given of how the boundary conditions can be used to determine the qualitative behavior of the diffracted intensities as functions of the magnitudes of the dynamical diffraction parameters. One new result of this approach is to show that for the case of two simultaneous reflections (the mixed Bragg–Laue case) certain geometries lead to zero intensity for the Bragg reflection.

It should be noted that it is only the existence of the boundary surface which is required for the present discussion, the structure in the diffracted intensities being related to bulk phenomena. The chemical state of a real crystal surface and the exact nature of the transition region between the interior and exterior of a crystal is known to strongly affect the details of the diffracted intensities, making LEED an important and useful tool for the study of surfaces. (See the bibliography in Dvoryankin and Mityagin, 1968.) However, such truly surface effects can only be discussed once the importance of the three-dimensional nature of the diffraction is recognized.

II. GLOSSARY

$\mathbf{a}_i$	Unit vector in the real lattice
$\mathbf{b}_j$	Unit vector in the reciprocal lattice
D	Tie point
E	Total electron energy
E_K	Eigenvalue of E whose eigenvector is the wave vector $\mathbf{K}$
$F_{O,G}(\mathbf{K}, E)$	The secular determinant
$\mathbf{G}$	Reciprocal lattice vector
$G(h, k, l)$	Reciprocal lattice point, where h, k, l are integers
H	Hamiltonian
$\mathbf{H}$	$\mathbf{H}^2=h^2+k^2+l^2$
$\mathbf{K}$	Electron wave vector in the crystal
$\mathbf{K}^r$	Real component of $\mathbf{K}$
$\mathbf{K}^i$	Imaginary component of $\mathbf{K}$
K_x	x Component of $\mathbf{K}$
$\mathbf{K}_{\|\|}$	Component of $\mathbf{K}$ parallel to the surface
$\mathbf{K}_G$	Wave vector associated with the $\mathbf{G}$th reflection, $\mathbf{K}_G=\mathbf{K}+\mathbf{G}$
$\mathbf{k}$	Electron wave vector in the vacuum, all components labeled as for $\mathbf{K}$
$\mathbf{k}_{\text{inc}}$	Wave vector of the electron incident on the crystal surface
N	Number of plane-wave states used in the expansion of the electron wave function
$U(\mathbf{X})$	Potential energy of the electron in the crystal
U_G	The $\mathbf{G}$th Fourier component of the potential energy

* The standard spherical diffraction coordinates in three dimensions are E, total incident energy; θ, angle of incidence with respect to the surface normal; φ, angle of orientation of the plane of incidence defined by the incident beam and the surface normal with respect to a fixed direction in the surface.

† The concept of the dispersion surface was originally derived for x rays by Ewald (1916).

‡ The relationship between total reflection (Bragg reflections) and bandgaps in the solid was first discussed by Morse (1930).

U_G^r, U_G^i	The real and imaginary components of U_G
$\mathbf{X}$, $\mathbf{R}$	Vector in real lattice
X	Coordinate in real lattice
ΔG	Energy denominator $=\mathbf{K}_G^2-E_K$
δG	$=\Delta G-U_0$
θ, φ	Angle of incidence (latitude) and azimuthal angle (longitude)
λ	Electron wavelength
$\mu(\mathbf{X})$	Periodic part of the Bloch function
μ	Absorption coefficient
ν	Surface normal
ϕ_G	Fourier coefficients of the wave function $\Psi_K(\mathbf{X})$
$\Psi(\mathbf{K}, \mathbf{R})$	Total wave function of the electron in the crystal
$\Psi_i(\mathbf{K}, \mathbf{R})$	Block wave associated with the ith tie point
$\Psi_G(\mathbf{K}, \mathbf{R})$	Wave field propagating in the direction of the reflection G
Ψ_{vac}	Total wave function of the electron in the vacuum

III. THEORY

A. Plane-Wave Expansion and the Secular Equation

Both band-structure and dynamical diffraction theory seek to determine the complete set of eigenfunctions of the Schrödinger equation for electrons in an infinite triperiodic crystal. As applied to diffraction, both theories have utilized plane-wave expansions of the crystal wave field. Formally this becomes the nearly free-electron approximation (NFEA) when the expansion is truncated.

The one-electron Schrödinger equation is

$$H\phi_K(\mathbf{X})=-\{\nabla^2+U(\mathbf{X})\}\phi_K(\mathbf{X})=E\phi_K(\mathbf{X}), \quad (1)$$

where $U(\mathbf{X})$, the potential energy of the electron in the three-dimensionally periodic crystal,*,† can be expressed as a three-dimensional Fourier sum:

$$U(\mathbf{X})=\sum_{\mathbf{G}} U_G \exp(-i\mathbf{G}\cdot\mathbf{X})=\sum_{\mathbf{G}} U_G \,|\, \mathbf{G}\rangle,$$

$$U_G=v^{-1}\int_v d^3X' \exp(i\mathbf{G}\cdot\mathbf{X}')U(\mathbf{X}'). \quad (2)$$

Here $\{\mathbf{G}\}$ is the set of reciprocal lattice vectors for the crystal space group, where $\mathbf{G}$ is the vector drawn from the origin of reciprocal space to the reciprocal lattice point $G(hkl)$.‡

The Bloch wave is expanded in a series of plane waves (momentum representation), most of whose terms will be small:

$$\phi_K(X)=\mu(\mathbf{X})\exp(i\mathbf{K}\cdot\mathbf{X})$$
$$=\sum_{\mathbf{G}}\phi_G\exp(i\mathbf{K}_G\cdot\mathbf{X})\equiv\sum_{\mathbf{G}}\phi_G\,|\,\mathbf{K}_G\rangle, \quad (3)$$

where $\mu(\mathbf{X})=\mu(\mathbf{X}+\mathbf{a})$ and $\mathbf{K}_G\equiv\mathbf{K}+\mathbf{G}$, $\mathbf{K}=\mathbf{K}^r+i\mathbf{K}^i$; therefore $\mathbf{K}_G{}^i=\mathbf{K}^i$ and $\mathbf{K}_G{}^r=\mathbf{K}^r+\mathbf{G}$. If Eqs. (2) and (3) are substituted into (1) and the scalar product $|\,\mathbf{K}_G\rangle$ is taken, Eq. (1) is turned into a set of linear homogeneous equations:

$$(\mathbf{K}_G^2-E_K)\phi_G+\sum_{\mathbf{H}}U_{H-G}\phi_H=0. \quad (4)$$

This basic set of equations is identical in band theory and dynamical diffraction theory.

If we now define the coefficient

$$\Delta_G\equiv(\mathbf{K}_G^2-E_K), \quad (5)$$

Eq. (4) can be written

$$\Delta_G\phi_G+\sum_{\mathbf{H}}U_{H-G}\phi_H=0. \quad (6)$$

Nontrivial solutions of Eq. (6) exist if and only if the secular determinant vanishes:

$$F_{0,G_1\ldots G_{N-1}}(\mathbf{K}, E)$$
$$=\begin{vmatrix} \Delta_0+U_0 & U_{G_2} & U_{G_2} & \cdots \\ U_{-G_1} & \Delta_{G_1}+U_0 & U_{G_2-G_1} & \cdots \\ U_{-G_2} & U_{G_1-G_2} & \Delta_{G_2}+U_0 & \cdots \\ \cdot & \cdot & \cdot & \cdot \\ \cdot & \cdot & \cdot & \cdot \\ \cdot & \cdot & \cdot & \cdot \end{vmatrix}=0. \quad (7)$$

Equation (7) is a $2N$th-order equation in the seven variables $\mathbf{K}^r$, $\mathbf{K}^i$, and E defining Δ_G, where N is the number of plane-wave states used in the expansion Eq. (3). The solutions to these coupled eigenvalue equations are the set of N eigenvalues $\{\Delta_0\}$ and the set of N eigenvectors $\{\phi_K{}^i\}$. Each eigenvector is an N-member column vector corresponding to a Bloch wave,

$$\phi_K{}^i(\mathbf{X})=\sum_{G=0}^{N-1}\phi_G{}^i\exp(i\mathbf{K}_G{}^i\cdot\mathbf{X}),$$

which has a fixed ratio of amplitudes $\phi_G{}^i/\phi_0{}^i$ determined by Eq. (6). The point of departure of the two theories is in assignment of Δ_G to $\mathbf{K}_G$ or E_K and arises from the boundary conditions usually associated with the problems considered by the two theories.

B. Comparison of Band Theory and Diffraction Theory

Band theory is usually concerned with internal electrons bound to the crystal with $E<0$. If one

* It is often easier to solve this equation if it is first transformed to a pseudowave equation (Harrison, 1956; Kittel, 1950; 1956; Heidenreich, 1950), where the pseudopotential $V(X)$ is substituted for $U(X)$. $V(X)$ is much weaker than the real potential, but has the same periodicity. The $\phi_K(\mathbf{X})$ then are the pseudowave functions which are smoother near the ion cores, but otherwise identical to the real wave functions; hence they can be expanded in a smaller number of plane waves; E_K are identical to the eigenenergies of the Schrödinger equation for conduction electrons. The choice of pseudopotential and the details of its construction do not alter or influence this discussion in any way.

† Atomic units are used so that $\hbar^2/2m=1$.

‡ $\mathbf{G}=2\pi\{h\mathbf{b}_1+k\mathbf{b}_2+l\mathbf{b}_3\}$, where $\mathbf{b}_i\cdot\mathbf{a}_j=\delta_{ij}$ and $\{\mathbf{a}\}$ is the set of basis vectors of the real lattice; h, k, l are integers.

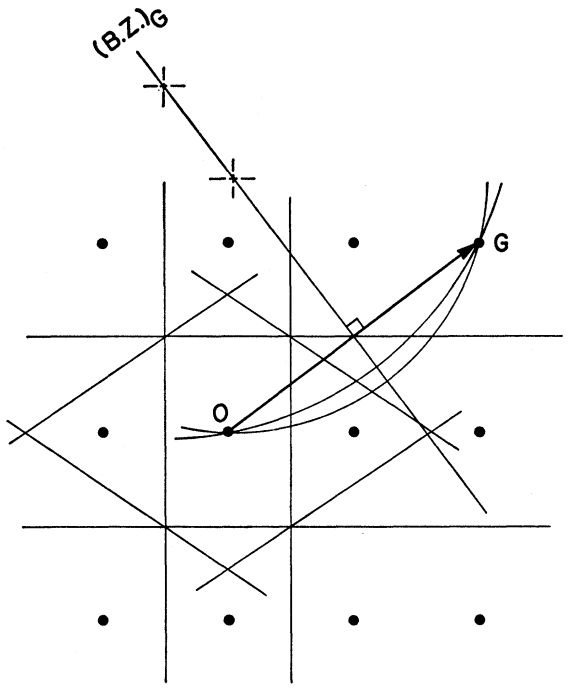

FIG. 1. A plane of the reciprocal lattice near the origin, showing the Brillouin zone boundary corresponding to the reflection **G**: The zone boundary **G** is the perpendicular bisecting plane of the vector **G**. Several other zone edges are also shown. The arc of the Ewald sphere of reflection passing through the origin and the reciprocal lattice point **G** is also shown, together with the center of the sphere, for two different energies. It can be seen from the construction that the Brillouin zone boundary (**G**) is just the locus of the center of all Ewald spheres passing through the origin and the reflection *G*.

considers the momentum **K** of the electron to be fixed, the crystal potential perturbs the energy of the electron so that an electron in momentum state $\mathbf{K}_G$ has energy $E_K=\mathbf{K}_G^2+\Delta_G$. It can be seen that once **K** is assumed, Eq. (7) reduces to an Nth-order equation in E with N roots, the N eigenvalues of the secular equation. These define the familiar bandgaps in the E-vs-**K** curve: The dispersion appears in E at constant **K**.

The dynamical theory of electron diffraction, on the other hand, is concerned with the behavior of external electrons injected into the crystal with fixed positive energy $E>0$. The unperturbed momentum **K** is therefore perturbed by the crystal potential and becomes $\mathbf{K}_G^2=E_K+\Delta_G$, and the dispersion appears in **K** at constant E. This can be compared, in principle, to the simple one-dimensional problem from elementary quantum mechanics

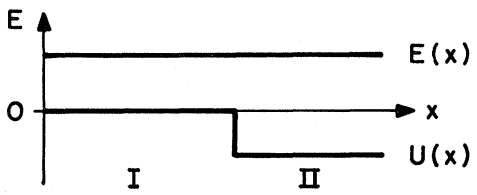

in which the total energy is a constant, but the kinetic energy and therefore the period of the wave function differs in the two regions of space I and II shown in the above diagram. Since the value of only one scalar variable, E, has been assumed in Eq. (7), the secular determinant described by the $2N$th-order equation in the variables $\mathbf{K}(K,\theta,\varphi)$ becomes the equation of $2N$ surfaces of constant energy in **K** space (in complex **K** space, six variables: $\mathbf{K}^r$; $\mathbf{K}^i$).

In the reciprocal lattice of the crystal, at a general point in space, **K**, the crystal periodicity causes no degeneracy if $|\mathbf{K}| \neq |\mathbf{K}+\mathbf{G}|$ for all **G**; under these conditions, in the nearly free-electron approximation, only one term in the plane-wave expansion has a large amplitude. In this case the equations become

$$\phi_K(\mathbf{X}) \approx \phi_0 |\mathbf{K}\rangle,$$

$$\Delta_0\phi_0+U_0\phi_0=0.$$

Therefore,

$$\Delta_0=-U_0=\mathbf{K}^2-E_K,$$

$$\Delta_0=(\mathbf{K}^r)^2-(\mathbf{K}^i)^2+2i\mathbf{K}^r\cdot\mathbf{K}^i-E_K. \tag{8}$$

In band theory the energy of the state with momentum **K** is

$$E_K=K_0^2+U_0, \tag{9}$$

whereas in dynamical diffraction theory (Ewald, 1916)* the momentum of the state of energy E_K is

$$|\mathbf{K}_0|=\pm(E_K-U_0)^{1/2}. \tag{10}$$

Since the average value of the potential energy of the electron in the crystal U_0 is negative, either E_K is decreased or $|\mathbf{K}|$ is increased with respect to the free-electron values.

The crystal symmetry causes a degeneracy, or an admixture of plane-wave states, wherever **K** is such that

$$|\mathbf{K}| = |\mathbf{K}+\mathbf{G}| = |\mathbf{K}_G|.$$

In band theory this is just the condition that **K** end on a Brillouin zone boundary (Kittel, 1950; 1956; Heidenreich, 1950); in dynamical diffraction theory this is the condition that G be on the Ewald sphere (Batterman and Cole, 1964; James, 1963; 1965). Geometrically these two conditions are identical: The Brillouin zone boundary defined by the perpendicular bisector of reciprocal lattice vector **G** is just the locus of centers of all Ewald spheres passing through the point G (Fig. 1).* In the nearly free-electron approximation, truncation of the infinite expansion is usually made by including only those G which are on or near to the Ewald sphere of reflection and have a radius equal to the average value of $|\mathbf{K}|$ for the crystal Bloch waves of energy E_K ($\mathbf{K}^2=E_K-U_0$) or those **G** corresponding to reflections whose Brillouin zone boundaries lie near the end of **K**.

* Simultaneous diffraction into more than one beam occurs if there is more than one reciprocal lattice point on the Ewald sphere or if **K** ends at the corner of a Brillouin zone.

For the case in which there is only one such **G**, Eqs. (4) become

$$(K_0^2-E_K)\phi_0+U_0\phi_0+U_G\phi_G=0,$$
$$(K_G^2-E_K)\phi_G+U_0\phi_G+U_G\phi_0=0, \quad (11)$$

where $U_G=U_{-G}$; i.e., a center of symmetry has been assumed.* This set of equations is usually written in the two cases as

(1) Band theory:

$$\{(\mathbf{K}_0^2+U_0)-E_K\}\phi_0+U_G\phi_G=0,$$
$$U_G\phi_0+\{(\mathbf{K}_G^2+U_0)-E_K\}\phi_G=0; \quad (12a)$$

(2) Diffraction theory:

$$\{\mathbf{K}_0^2-(E_K-U_0)\}\phi_0+U_G\phi_G=0,$$
$$U_G\phi_0+\{\mathbf{K}_G^2-(E_K-U_0)\}\phi_G=0. \quad (12b)$$

The secular equations for the eigenvalues in the two theories are then

$$\begin{vmatrix}(\mathbf{K}_0^2+U_0)-E_K & U_G\\ U_G & (\mathbf{K}_G^2+U_0)-E_K\end{vmatrix}=0; \quad (13a)$$

$$\begin{vmatrix}\mathbf{K}_0^2-(E_K-U_0) & U_G\\ U_G & \mathbf{K}_G^2-(E_K-U_0)\end{vmatrix}=0. \quad (13b)$$

In band theory this secular equation leads to the familiar energy bandgap ($E_K=\mathbf{K}_0^2+U_0+U_G$) at the Brillouin zone boundary ($\Delta_0=\Delta_G$), where purely real **K** solutions are forbidden, and to the dispersion in **K** of E leading to effective mass formulas. Wave functions having complex **K** are allowed everywhere, including the gap (Heine, 1964). The necessity of maintaining finite electron densities everywhere requires that such wave functions have nonzero amplitudes only around impurities or near surfaces. Figure 2 shows the energy as a function of $\mathbf{K}_0$ (complex). [The analytic properties of the energy and Bloch functions as functions of complex **K** are extensively discussed elsewhere (Blount, 1962; Stern, 1967; Kohn, 1957; Krieger, 1966; Heine, 1965), including in particular the branch points on the complex **K** plane and the proper connection of the energy band sheets in complex space.] The coordinates of Fig. 2 are chosen such that $\mathbf{K}_2$ is orthogonal to $\mathbf{K}_1$. (This is not the usual one-dimensional K-vs-E diagram where K^r is parallel to K^i.) The reason for this choice is to demonstrate that in the case where $\mathbf{K}_2{}^r$ lies in the surface and $\mathbf{K}_1{}^i$ is directed normal to the surface, there is an infinite allowed set of exponentially decaying solutions having a $\mathbf{K}^i$ vector normal to a particular propagating solution.

In dynamical diffraction theory, Eq. (13b) is the equation of a constant-energy surface in complex **K**

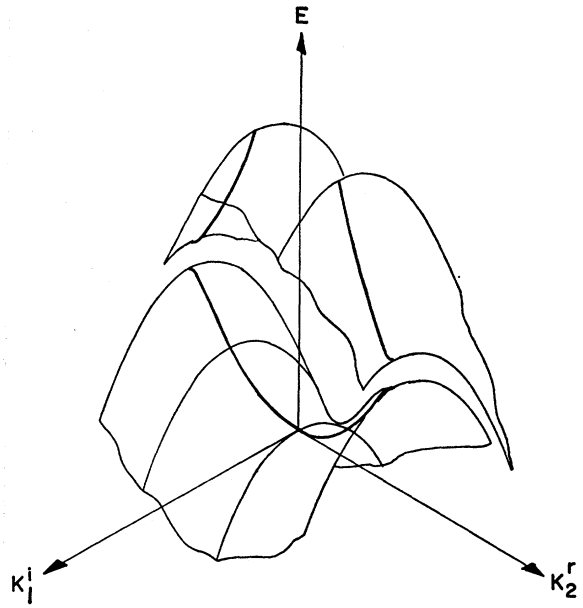

FIG. 2. Solution of Eq. (13b) for $(E, \mathbf{K}_2{}^r, K_1{}^i)$. In this drawing, the coordinates are chosen such that $\mathbf{K}_1{}^i$ is orthogonal to $\mathbf{K}_2{}^r$. In order to demonstrate the fact that for an arbitrary value of $\mathbf{K}_2{}^r$, for example, one corresponding to a wave traveling in the plane of the surface, there are an infinite number of imaginary solutions $\mathbf{K}_1{}^i$ which decay away from the surface into the crystal. This is not the section usually shown (where the real and imaginary components of **K** are chosen parallel to each other).

space known as the dispersion surface. Each point on the surface corresponds to a pair of allowed **K** vectors, one drawn to (0) and the other to (G). The eigenstate of energy E_K corresponding to that point is described by an eigenfunction which is the sum of two plane waves whose wave vectors are the aforementioned pair and whose amplitudes, ϕ_0 and ϕ_G, are determined from Eq. (12b) by substituting the appropriate pair of wave vectors. Figure 3(a) shows the constant-energy surface in the region of the dispersion in **K** due to the single perturbation U_G. Equation (13b) can be written

$$(\mathbf{K}_0^2-E')(\mathbf{K}_G^2-E')=U_G^2: \quad E'\equiv E-U_0,$$
$$\Delta_0'\Delta_G'=U_G^2>0, \quad (14)$$
$$\therefore \operatorname{sgn}\Delta_0'=\operatorname{sgn}\Delta_G',$$

which is the equation of a hyperbola (in $\mathbf{K}_0^2$ and $\mathbf{K}_G^2$) asymptotic to spheres of radius **K** about 0 and G, shown by the heavy lines in Fig. 3(a).

The totality of solutions of the secular equation represents a surface in $(E, \mathbf{K})$ complex hyperspace. This seven-dimensional surface $(E, \mathbf{K}^r, \mathbf{K}^i)$ is called the dispersion hypersurface. A section of this hypersurface at constant E and constant $\mathbf{K}^i$ ($\mathbf{K}^i=0$) is the familiar dispersion surface of dynamical diffraction theory. A section at constant θ, ϕ and $\mathbf{K}^i=0$ is the familiar energy dispersion of band theory. These sections are shown in Figs. 3(a) and 3(b), respectively. The magnitude of the dispersion in **K**

* In a higher-order approximation, the weak beams ($\mathbf{K}_G^2+U_0-E_K>0$) can also be included.

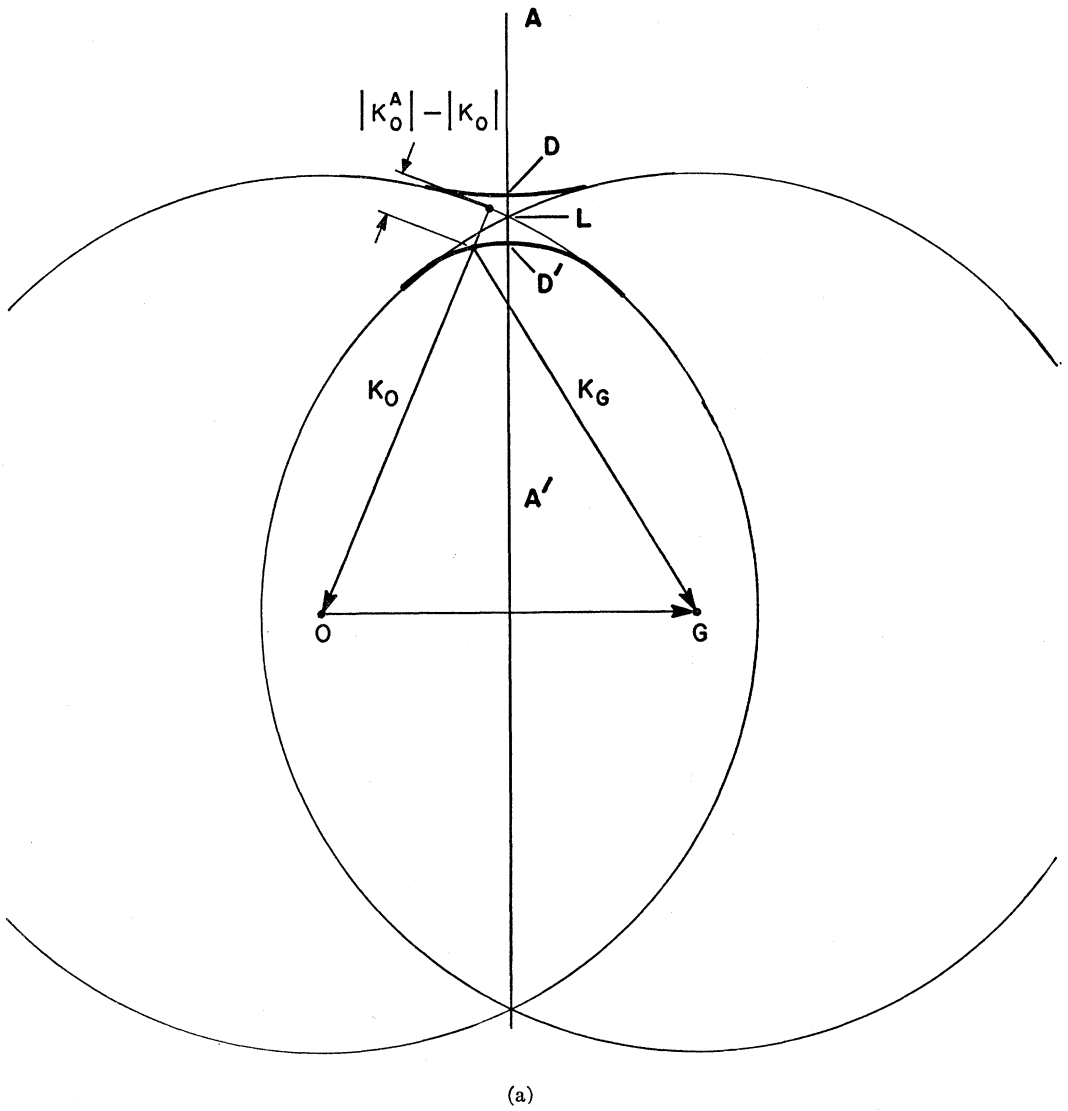

(a)

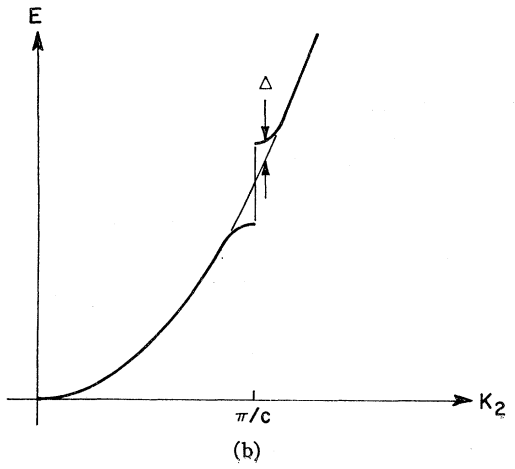

(b)

FIG. 3. (a) Dispersion sheets of real **K** (the constant-energy surfaces) at an energy $|\mathbf{K}_0|^2$ which lies in the center of the bandgap associated with the reflection G. AA' is the Gth Brillouin zone boundary and is called the diameter line in diffraction theory. D and D' are called the diameter points. The intersection of the free-electron spherical constant-energy surfaces, L, is known as the Laue point. (b) Energy dispersion diagram at the first Brillouin zone boundary. The dispersion in energy at the Brillouin zone boundary is measured from the parabolic free electron surface.

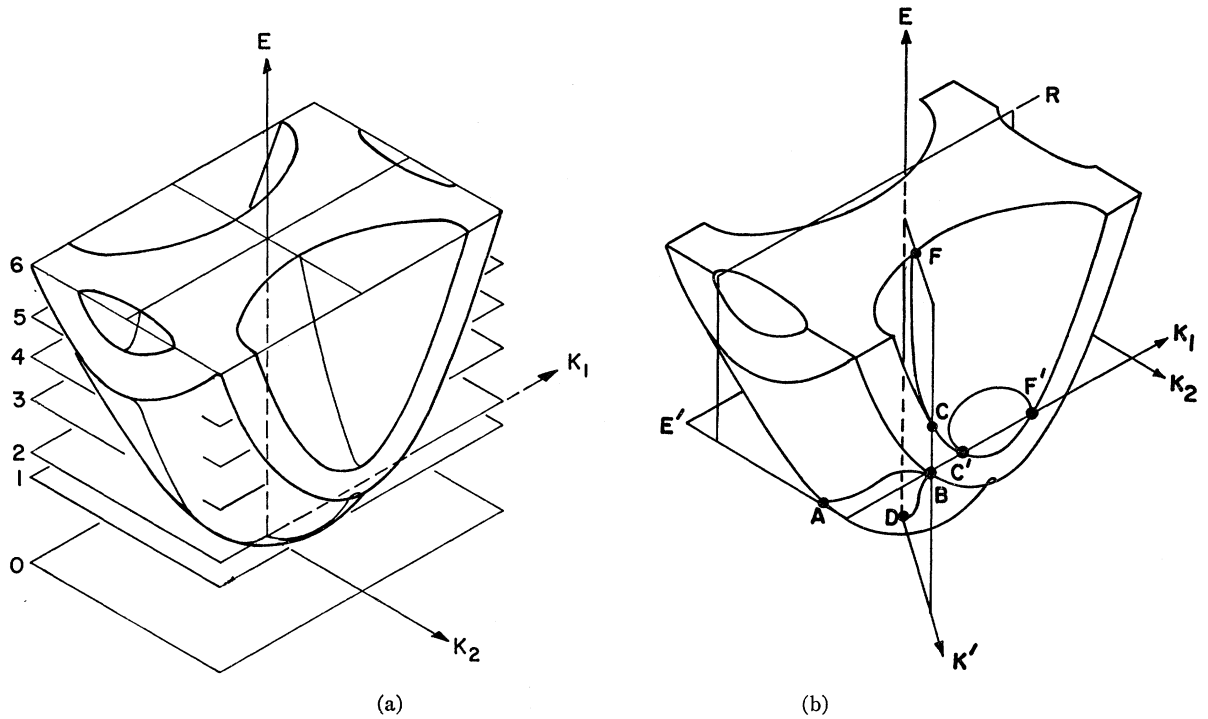

FIG. 4. (a) A three-dimensional (E, $\mathbf{K}_1^r$, $\mathbf{K}_2^r$) isometric view of the dispersion hypersurface in the first Brillouin zone. (b) The outline of Fig. 4(a), showing the intersection of the dispersion hypersurface with a constant-energy plane ($\mathbf{K}_1$, $\mathbf{K}_2$) and with an arbitrary $\mathbf{K}$ plane (E, $\mathbf{K}'$). The point B shown lies in both these planes. If these planes are considered to be those of Figs. 3(a) and 3(b), then it can be seen that the figures can have a point on the edge of the bandgap in common. Traversing the gap from this point in one plane is not equivalent to traversing it in the other plane from the same point, since the points C, C' are not equivalent.

at constant E and in E at constant $\mathbf{K}$ is indicated.

The dispersion hypersurface is a general property of the crystal, describing as it does the energy of the Bloch wave at any point in $\mathbf{K}$ space. The problem reduces to the accurate determination of the form of the Bloch wave (NFEA, OPW, etc.) at any point on the hypersurface.

A three-dimensional section of this surface (E, $\mathbf{K}_1^r$; $\mathbf{K}_2^r$), chosen so as to illustrate the connection between the two standard diagrams, is shown in Fig. 4(a). In Fig. 4(b), the outline of the dispersion hypersurface of Fig. 4(a) is shown together with the trace (near the Brillouin zone boundary) of the surface ($ABC'F'$) on a plane of $E=E'=$ const and the trace ($DBCF$) on a plane of arbitrary $\mathbf{K}=\mathbf{K}'=$ const. These two planes contain the common point B which lies on the edge of the gap. If the planes indicated are the planes of Figs. 3(a) and 3(b), then the relationship between the dispersion in E and in $\mathbf{K}$ can be seen. Traversing the gap at constant energy (from B to C') is not equivalent to traversing the gap at constant $\mathbf{K}$ (from B to C).

In Fig. 5(a), constant-energy slices of Fig. 4(a) in the first Brillouin zone are taken at the levels indicated. These are constructed following the rules usually associated with the drawing of the dispersion surface in the dynamical theory (Batterman and Cole, 1964; James, 1963; 1965) [the Harrison construction (Harrison, 1956) for nearly free-electron constant-energy surfaces]. The usual band diagrams are indicated on the $E-\mathbf{K}_1$ and $E-\mathbf{K}_2$ planes of Fig. 4(a), illustrating the bandgaps in the directions $\mathbf{K}_1$ and $\mathbf{K}_2$. Figure 5(b) shows these band diagrams drawn in the series of planes having orientations between that of $E-\mathbf{K}_1$ and $E-\mathbf{K}_2$, in the quadrant $\mathbf{K}_1-\mathbf{K}_2$ of Fig. 4(a). Figure 5(c) shows the intersection of the surface of Fig. 4(a) with the plane $\mathbf{K}_2=$ constant, chosen at the level R shown in Fig. 4(b). The bandgap at the first Brillouin zone boundary is shown.

IV. BOUNDARY CONDITIONS IN ELECTRON DIFFRACTION

A. Theory

If a crystal surface is introduced into the problem, the conditions existing on the boundary as defined by a given experiment determine in a self-consistent way which Bloch waves allowed in the bulk are excited. The presence of a surface admits both the real and complex $\mathbf{K}$ solutions, the latter decaying normally from the surface.

The boundary conditions require:

(a) conservation of energy,

(b) conservation of momentum parallel to the surface,

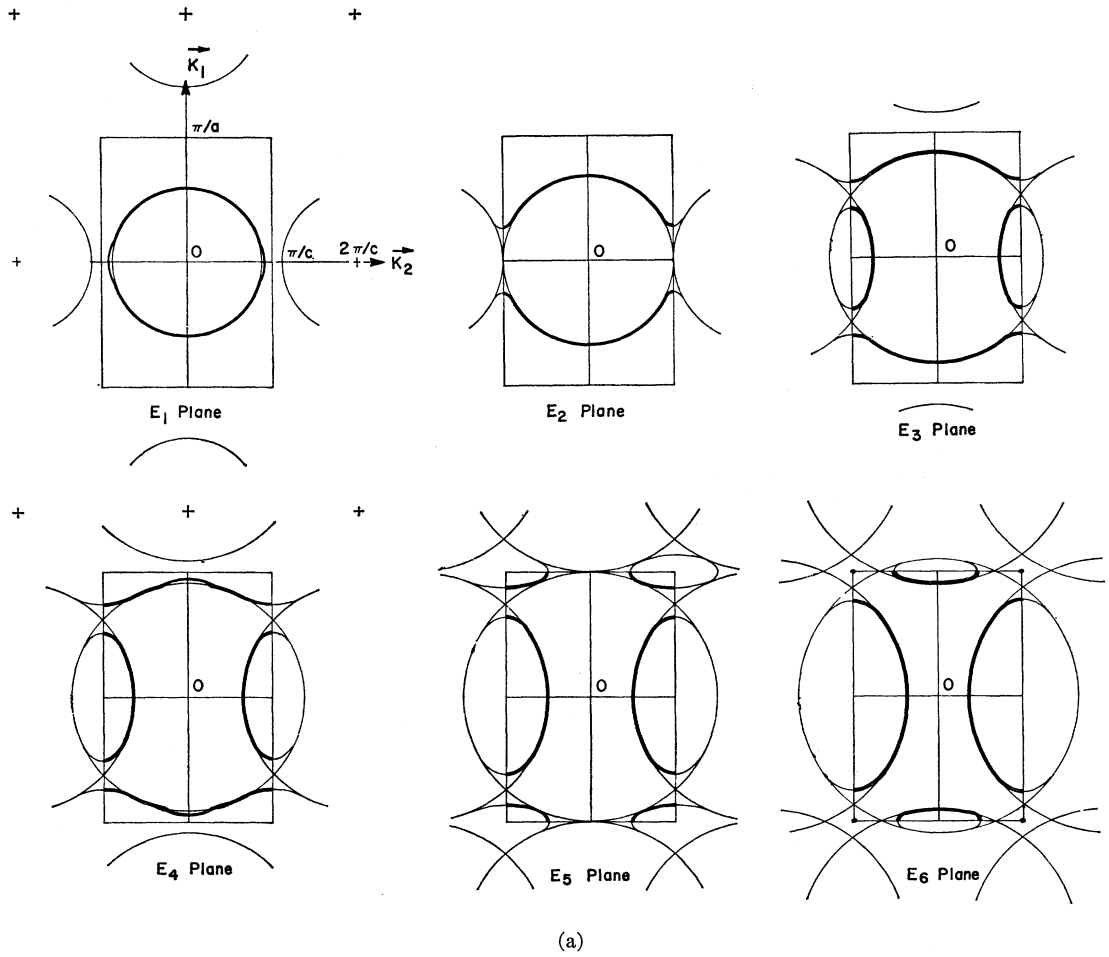

(a)

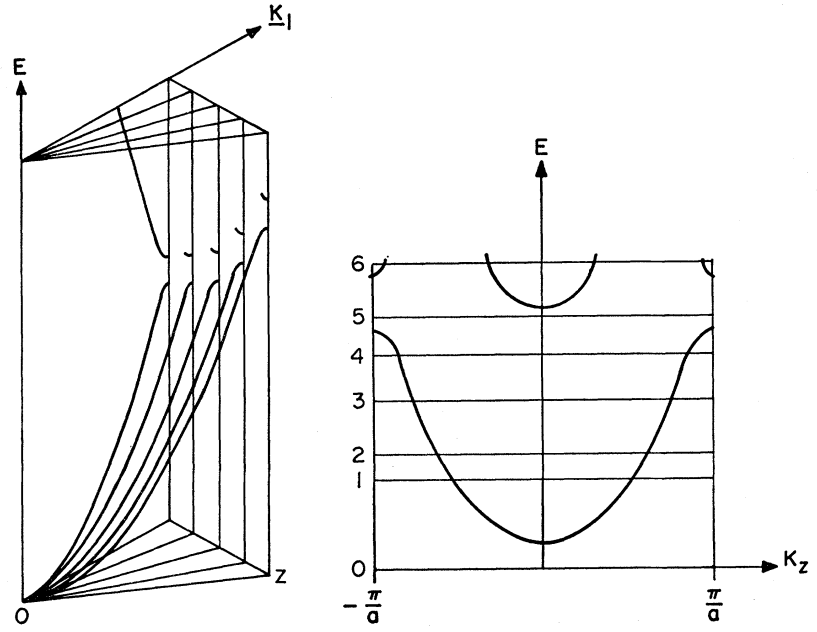

(b) (c)

FIG. 5. (a) Constant-energy sections of Fig. 4(a), taken at the levels E_1–E_6 indicated in Fig. 4(a), constructed in the manner suggested by dynamical diffraction theory. (b) E-vs-$\mathbf{K}$ band diagrams, in a series of planes having orientations between $E-\mathbf{K}_1$ and $E-\mathbf{K}_2$, in the quadrant $\mathbf{K}_1-\mathbf{K}_2$ of Fig. 4(a). (c) Section of Fig. 4(a), taken in the plane $\mathbf{K}_2=$const at a position R shown in Fig. 4(b). The drawings of Figs. 5(a) and 5(c) are just the solutions of Eq. (13b) for $(\mathbf{K}_1{}^r, \mathbf{K}_2{}^r)$ and $(\mathbf{K}_1{}^r, E)$, respectively.

(c) continuity of the total wave function and its normal derivative at the surface,*

(d) finite electron densities everywhere.

For the plane-wave description to be valid, condition (c) requires that the expansion include solutions for both real and complex **K**; i.e., the evanescent waves in both the vacuum and the crystal must always be taken into account for the proper matching of the wave field at the surface.

The last condition (d) requires that the complex solutions have imaginary parts normal to the surface only, i.e., $\mathbf{K}_i = K_i \hat{z}$. Since this fact is common to all experiments at a single surface ($z=0$), the constraint surface in imaginary space is the plane $K_x^i = K_y^i = 0$ for all experiments.

Conditions (a) and (b) are used to determine the proper set of eigenfunctions excited in the crystal, and condition (c), to determine the relative amplitudes of each of the eigenfunctions in the crystal and in the vacuum. The incident beam is assumed to have unit amplitude, and there can be no other waves in the vacuum traveling towards the crystal. Condition (d) therefore prohibits the excitation in a real, semi-infinite crystal with absorption of Bloch waves having a net electron flow towards the entrance surface, since this would require an infinite source deep within the crystal.†

The selection of the set of excited eigenfunctions in the crystal satisfying the first two boundary conditions is formally accomplished by determining the intersection between the dispersion hypersurface and the constraint surface in a given experiment. To determine which solutions of real **K** satisfy the last boundary condition, it is necessary to establish the direction of electron flow parallel to the velocity vector of the Bloch wave associated with each point on the dispersion surface. It can easily be shown (Peierls, 1929; Sommerfeld and Bethe, 1933) that the velocity of the Bloch wave $\langle \phi_K(\mathbf{X}) \mid \mathbf{v} \mid \phi_K(\mathbf{X}) \rangle$ always has a direction perpendicular to the constant-energy dispersion surface $[\langle v \rangle = \nabla_K E/(2m)^{1/2}]$ (see Appendix); hence not all eigenfunctions can be excited in a given experiment.

In the following we will discuss the geometrical conditions imposed in real $\mathbf{K}-E$ space in those diffraction experiments which determine simple constraint surfaces. It is to be emphasized, therefore, that in addition to the Bloch waves excited with real **K** there are those which satisfy the combination of constraints in real **K** space along the K_z^i axis of complex space.

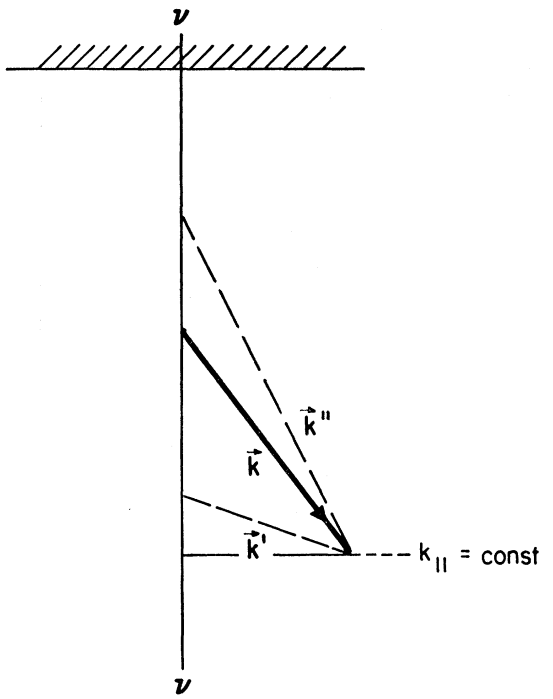

FIG. 6. The surface normal ν drawn through the end of the incident vacuum **k** vector. It can be seen that all the vectors drawn from the origin to the surface normal have the same components of **k** parallel to the surface. This is the construction which allows the geometrical determination of all the points on the dispersion surface which correspond to plane waves satisfying this boundary condition.

There exist three methods of systematically scanning the **K** vector of the incident wave through reciprocal space, varying only one of the diffraction parameters at a time: (1) The energy E of the incident electron beam may be varied while either keeping the direction (θ, ϕ) of the incident beam constant (pseudorocking curve) or maintaining $\mathbf{K}_{||}$ constant. (2) The angle of incidence, θ, may be varied while keeping the energy E and orientation ϕ constant (rocking curve). (3) The crystal can be rotated about the surface normal, maintaining the angle of incidence θ and the energy E, constant (rotation diagram). If a Bragg reflection appears in the specularly reflected beam in the third case, that reflection is maintained during the rotation.

It is appropriate to first discuss constant-energy experiments, cases (2) and (3). Here the obvious constraint surface is the surface $E=E_{\text{inc}}$. The intersection with the dispersion hypersurface is the constant-energy dispersion surface, two-dimensional sections of which were shown in Fig. 5(a). From this constant-energy set of Bloch waves the appropriate excited subset is that which conserves momentum parallel to the surface. The constraint surface defined by this condition is generated by the locus of the surface normal through the end of the vacuum **k** vector ($\mathbf{K}_{||}=\mathbf{k}_{||}$) (Fig. 6). In the rocking-curve experi-

* For a finite crystal these same boundary conditions apply at the exit surface with the additional condition that there are no incoming waves from the vacuum at that surface.

† In the problem of a finite crystal, all surfaces must be considered, requiring the generalization to seven-dimensional space since the exponential decay is in three independent directions. In the case of a thin crystal, the direction of electron propagation is no longer restricted, since waves propagating towards the entrance surface, even though they are attenuated by the crystalline absorption, always are of finite amplitude within the finite crystal.

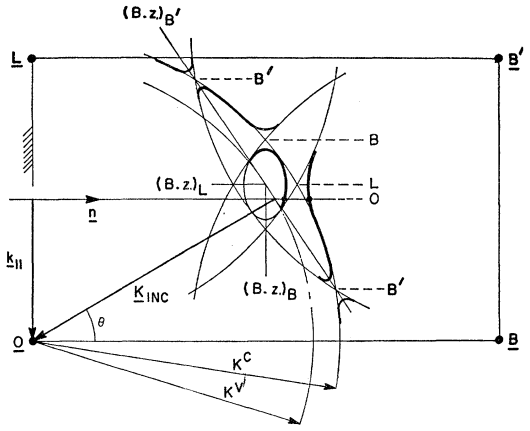

FIG. 7. The constant-energy dispersion surface in the region of three reflections, L, B, B'. The incident direction of the vacuum wave vector $\mathbf{k}_{inc}$ is shown, as is the orientation of the surface and the surface normal. The points B', L, B, B' indicate the position of the Brillouin zone boundary for those reflections.

ment the locus is the plane of incidence (ϕ=const). In the rotation-diagram experiment the locus is the cylinder whose axis is the surface normal and whose radius is $\mathbf{K}_{||}$.

Consider the generation of the rocking curve in detail. Figure 7 shows the intersection of the plane of incidence with the constant-energy surface: a section of the spherical constant-energy surface in the vacuum (radius $k^v=E^{1/2}$) is also indicated. The plane of the surface is indicated at the origin, properly orientated in reciprocal space. The incident vacuum wave vector $\mathbf{k}_{inc}$ is drawn at the proper angle of incidence, θ, with respect to the surface normal. A line parallel to the surface normal drawn through the end of this vector will then intersect the constant-energy surface at those $\mathbf{K}$ (called tie points) such that the Bloch waves associated with those points satisfy the boundary conditions (a) and (b). The rocking curve is then generated as θ is varied, moving the points of intersection from 0 to L to B to B'.

The position of the Brillouin zone boundary for the reflections (B'), (L), (B) are shown at the points B', L, and B. As the incident direction is varied, the successively excited crystal wave vectors, $\mathbf{K}_L$, $\mathbf{K}_B$, and $\mathbf{K}_{B'}$, are drawn from the tie points to the reciprocal lattice points $L(mno)$, $B(hkl)$, and $B'(rst)$, respectively. A reflection is designated to be of the Laue type when the diffracted wave vector is directed into the crystal (forward scattering or transmission); a Bragg reflection occurs when the wave vector is directed towards the vacuum (back scattering or total reflection). For the orientation of the surface normal shown in Fig. 7, the points $B(hkl)$ and $B'(rst)$ correspond to Bragg reflections and $L(mno)$ corresponds to Laue reflections. These reflections are excited for orientations of the incident $\mathbf{K}$ vector such that the surface normal passes through the regions of the dispersion surface near B', B, and L. It should be noted that in the region of B, no traveling waves are excited and the incident beam suffers total reflection. On either side of the two-beam Bragg reflection, the surface normal cuts the dispersion sheet at two points. In a real, semi-infinite crystal, only the tie point corresponding to an energy flow into the crystal has a physical meaning.

There are two obvious experiments in which the energy may be varied. In one case, the parallel component of $\mathbf{K}$ ($\mathbf{k}_{||}$) is maintained constant, resulting in a planar constraint surface; its interaction with the dispersion hypersurface is the energy-vs-K_z band structure, a simplified plot of which is shown in Fig. 5(c). This experiment is difficult to perform, however, since to maintain $\mathbf{k}_{||}$ constant while varying $\mathbf{k}_z$ requires an accurate simultaneous variation of both the magnitude and direction of the incident beam $\mathbf{k}^{inc}$. The other experimental condition, in fact the one usually chosen in LEED measurements, is maintenance of the incident direction of $\mathbf{k}^{inc}$ constant and variation of the energy. In this case the constraint surface is the plane of incidence, and the region of the dispersion surface near to the intersection with the surface normal through the end of $\mathbf{k}^{inc}$ must be reconstructed at each energy. Thus, while the second method is experimentally easier, an analytical description of the trace of the intersection of the dispersion surface with the constraint surface is difficult to formulate. The geometrical interpretation is made in the same way as for the rocking curve.

After the excited set of Bloch waves from the intersection of the constraint and dispersion surfaces have been determined, the amplitudes of the Bloch waves for any experiment are obtained from the conditions of continuity of the wave function and its normal derivative. Each eigenfunction associated with the ith tie point* can be written as

$$\Psi_i(\mathbf{K},\mathbf{R})=\sum_G \phi_G{}^i \exp(i\mathbf{K}_G{}^i\cdot\mathbf{R}),$$

and the total wave function becomes

$$\Psi=\sum_i C_i\Psi_i(\mathbf{K},\mathbf{R}). \tag{15}$$

The wave field Ψ_G, propagating in the direction of the reflection G,† can be written as

$$\Psi_G=\sum_i C_i\phi_G{}^i \exp(i\mathbf{K}_G{}^i\cdot\mathbf{R}), \tag{16}$$

and the total wave function can then be written

$$\Psi=\sum_G \Psi_G.$$

The C_i are determined from the boundary conditions which can be written as

$$\Psi_{vac}\,|_{z=0}=\sum_i C_i\Psi_i(\mathbf{K},\mathbf{R})\,|_{z=0}, \tag{17a}$$

$$\partial\Psi/\partial z_{vac}\,|_{z=0}=\sum_i C_i(\partial\Psi_i/\partial z)\,|_{z=0}. \tag{17b}$$

* Only those tie points associated with allowed direction of electron transport are included.

† It is proposed to call this the Ewald wave.

Since Ψ is expanded in a Fourier series, Eqs. (17) can be applied term by term. In the vacuum, $U=0$ and solutions of Eq. (1) are plane waves of real and complex $\mathbf{k}$. At the boundary, therefore, in addition to the vacuum plane waves usually considered, there will be evanscent waves with amplitudes decaying away from the surface into the vacuum. The imaginary part of any complex $\mathbf{k}$-plane wave of real energy must be normal to the real $\mathbf{k}$, and thus the only allowed evanscent waves in the vacuum have real $\mathbf{k}$ parallel to the surface.*

B. Experimental Conditions

The intensity of any reflection from a given surface is uniquely determined by the values of all three incident diffraction parameters. In each experiment the boundary conditions select different sets of excited eigenfunctions, and some selected by one method will never be selected by the others unless the initial conditions of the several scans are deliberately chosen so as to excite the same tie point in hyperspace. Even if the same point is excited in the different experiments, the sequence of adjacent points excited during the scan will usually be different [see Fig. 4(b)]; thus the comparison between measurements is difficult. In dynamical theory, the object of both theory and experiment is to determine the effects of simultaneous diffraction. Because it is easy to vary the energy in the apparatus commonly employed in LEED, the technique of measuring intensity vs energy has been almost exclusively in LEED. In such a measurement, vast areas of the dispersion hypersurface will not be excited. In particular for any incident direction of high symmetry, no matter how high the energy is allowed to become, the sphere of reflection will never excite those points lying in a dense reciprocal lattice plane passing through the origin and normal to the incident beam.

Recent experiments in this laboratory have indicated that it is the excitation of precisely these low-index Laue reflections which are responsible for much of the anomalous structure observed in the reflected intensity (Stern and Taub, 1968; Stern, Taub, and Gervais, 1969; Stern, 1968) in typical LEED measurements. There the incident direction is not one of high symmetry, but is chosen to be several degrees from the surface normal (which is usually a low-index direction) in order to allow observations of the specularly reflected beam. These small deviations from directions of high symmetry are sufficient to excite low-index Laue reflections. (In Sec. V of this paper we discuss two highly simplified models of these interactions.)

For a cubic crystal, the Fourier coefficients of the potential, U_H, decrease with increasing values of $H^2=h^2+k^2+l^2$,† and are therefore largest for low-index reflections which are strong. In order to excite low-index reflections, it is necessary to move the incident beam away from one of the high-symmetry directions of the crystal. When the incident beam is parallel to a low-index direction, then the symmetry of the reciprocal lattice makes all simultaneous reflections degenerate, insomuch as symmetrical reciprocal lattice points will always be excited simultaneously. If the incident beam is moved away from the low-index direction to excite a strong forward-diffracted beam, then the degeneracy of the simultaneous reflections is removed, and the intensity measurements are characterized by a manifold increase in the fine structure observed. This is true in the nearly free-electron model; the effect of the degeneracy and its removal become more severe in any model containing stronger interactions. A detailed discussion of the fine structure observed in the three types of measurements described above will appear elsewhere.

V. DYNAMICAL INTERACTIONS IN THE TWO- AND THREE-BEAM CASES

A. Introduction

In order to illustrate the effects of the dynamical interactions between the several plane-wave components of the Bloch waves, it is useful to discuss several simple multiple-beam cases.

For the two-beam case ($N=2$), when a Laue reflection is excited symmetrically [point L of Fig. 3(a)], the two forward-scattered plane waves have equal amplitudes, but are not colinear. This gives rise to a traveling wave moving parallel to the Brillouin zone boundary into the crystal and a standing wave normal to the Brillouin zone boundary. The standing wave is associated with a periodic variation of the wave-field amplitude in the crystal (pendellösung) which can be observed in conventional electron transmission microscopy, as extinction contours in thin, wedge-shaped crystals. In a thick crystal, these interactions occur only for the forward-scattered beam which is not observed in low-energy electron diffraction.*

The excitation of a Bragg reflection in a semi-infinite crystal where only a single tie point can be excited is accompanied by a single-crystal plane wave

* For a plane wave in the vacuum: $\nabla^2\phi=E\phi$ and $\phi=\exp(i\mathbf{k}\cdot\mathbf{R})$. Thus $(\mathbf{k}^r)^2-(\mathbf{k}^i)^2+2i\mathbf{k}^r\cdot\mathbf{k}^i=E$; therefore $2i\mathbf{k}^r\cdot\mathbf{k}^i=0$, and $(\mathbf{k}^r)^2-(\mathbf{k}^i)^2=E$.

† For a discussion of structure amplitudes see Chap. 3 of Vainstein (1964).

* Detailed discussions of the two-beam case for x rays (Batterman and Coles, 1964; James, 1963, 1965) and electrons (Hashimoto, Howie, and Whelan, 1962) appear in the literature. The importance of the forward-scattered beam for LEED has been discussed in terms of the different absorption associated with the plane waves for each dispersion sheet (Taub and Stern, 1968; Stern and Taub, 1968). The details of the wave-field amplitudes and the dispersion surface for high-energy electron diffraction for the N-beam case have been treated in the literature [Lehmpfuhl and Reiszland, 1968; Fues, 1936; 1943; Wagner, 1951; Penning and Polder, 1968]. Discussions of the relative wave-field amplitudes for the three-beam Laue case here also appeared for high-energy electrons (Niehrs, 1954a; 1954b; Moliere and Niehrs, 1954) and for x rays (Ewald and Heno, 1968; Heno and Ewald, 1968; Penning, 1968).

scattered towards the vacuum at the edge of the gap and decaying evanesent crystal wave in the gap. The shape of this Bragg reflection is well known for the case where there is no absorption (Kronig and Penny, 1931). In a finite crystal, pendellösung is expected in the Bragg reflection because in this case both tie points can be excited.

The consideration of the three-beam case will allow a contrast to be made between the dynamical predictions of the two approximations. However, the three-beam approximation is just that: an attempt to expand each of the crystal Bloch waves in terms of three plane waves. This is best seen by rewriting Eq. (4) as

$$\phi_G = \sum_H [U_{H-G}\phi_H/(K_G^2 - E_K)]$$

and noting that the expansion contains terms which are large only when the energy denominator (Δ_G) is approximately zero. For most experiments at moderate or high energies, for arbitrary values of the diffraction parameters, this approximation ($N=3$) is not valid because of the existence of other strongly excited reflections. It is only by careful choice of the magnitude and limitation of the range of the diffraction parameters that an approximate three-beam situation can be excited.

The following section is therefore intended only as a guide to help in the understanding of the role that the boundary conditions play in determining the relative plane-wave amplitudes and hence the diffracted intensities during an experiment. The use of the three-beam approximation will permit a qualitative understanding of the physical origin of certain phenomena which are frequently observed in the experimentally determined reflected intensities.

B. The Two-Beam Case

It is instructive to first examine the dispersion surface in a region where the two-beam approximation is valid. The Bragg–Laue conditions are fulfilled exactly at the intersection of the two spherical free-electron constant-energy surfaces. This point is known as the Laue point of the reflection [point L in Fig. 3(a)]. If the surface normal drawn through the end of $\mathbf{k}^{\text{inc}}$ passes through this point, then the reciprocal lattice point of the reflection lies on the Ewald sphere. That is the case for the orientation of the incident wave vector indicated by the points L and B and B' in Fig. 7. The relative amplitude of the plane wave at a tie point on a particular dispersion sheet is inversely proportional to the distance between the tie point and the Laue point for that reflection (Bethe, 1928). If no tie point is excited, as in a pure Bragg reflection, the incident beam is totally reflected across the region of the gap.*

* The evanescent wave amplitude is constant across the gap, providing for a constant reflection coefficient in this region.

The surface normal parallel to the Brillouin zone boundary (L), passing through the Laue point, intersects the dispersion surface at the symmetrical tie points [D and D' of Fig. 3(a)] which are known as the diameter points. In a real crystal where inelastic processes must be considered, the waves associated with each sheet of the dispersion surface propagate with different absorption coefficients. The wave associated with the dispersion sheet farthest from the origin has an absorption coefficient larger than the average value, and the wave associated with the dispersion sheet nearest to the origin has an absorption coefficient lower than average; at the diameter points, the difference between the two absorption coefficients is a maximum, the one wave being anomalously absorbed, the other being anomalously transmitted [Borrmann effect (1941)].

In the multiple-beam case it is possible to estimate the relative strength of the plane waves associated with each tie point by considering each reflection of the two-beam approximation. It must be remembered, however, that all the excited dispersion sheets contributed to each reflection, so that only a very qualitative description of the reflected intensities can be given.

C. The Three-Beam Case

The matrix equation describing the three-beam case is

$$\begin{pmatrix} \Delta_0 - U_0 & U_{G_1} & U_{G_2} \\ \mathbf{U}_{-G_1} & \Delta_1 - U_0 & U_{G_2-G_1} \\ \mathbf{U}_{-G_2} & U_{G_1-G_2} & \Delta_2 - U_0 \end{pmatrix} \begin{pmatrix} \phi_0 \\ \phi_1 \\ \phi_2 \end{pmatrix} = 0.$$

Thus the equation of the dispersion surface becomes

$$F_{0,G_1,G_2}(\mathbf{K}, E) = \delta_0\delta_1\delta_2 - [U_{G_2-G_1}U_{G_1-G_2}\delta_0 + U_{G_1}U_{-G_1}\delta_2 + U_{G_2}U_{-G_2}\delta_1] + [U_{G_1}U_{-G_2}U_{G_2-G_1} + U_{-G_1}U_{G_2}U_{G_1-G_2}] = 0, \quad (18)$$

where $\delta_0 = \Delta_0 - U_0 = \mathbf{K}_0^2 - \mathbf{K}^2$ and $\mathbf{K}^2 = E_K - U_0$.

The ratios of the field amplitudes of the Bloch waves are

$$\frac{\phi_1}{\phi_0} = \frac{\begin{vmatrix} \delta_0 & U_2 \\ U_{-2} & \delta_2 \end{vmatrix}}{\begin{vmatrix} U_1 & U_2 \\ U_{2-1} & \delta_2 \end{vmatrix}} = \frac{\begin{vmatrix} \delta_0 & U_2 \\ U_{-1} & U_{2-1} \end{vmatrix}}{\begin{vmatrix} U_1 & U_2 \\ \delta_1 & U_{2-1} \end{vmatrix}}, \quad (19a)$$

$$\frac{\phi_2}{\phi_0} = \frac{\begin{vmatrix} \delta_0 & U_1 \\ U_{-1} & \delta_1 \end{vmatrix}}{\begin{vmatrix} U_1 & U_2 \\ \delta_1 & U_{1-2} \end{vmatrix}} = \frac{\begin{vmatrix} \delta_0 & U_1 \\ U_{-2} & U_{2-1} \end{vmatrix}}{\begin{vmatrix} U_1 & U_2 \\ U_{2-1} & \delta_2 \end{vmatrix}}, \quad (19b)$$

where the indices 0, 1, 2 refer to the reflections $O(000)$, $B(khl)$ and $L(mno)$, respectively.

There is no loss of generality and the geometry is considerably simplified if the reciprocal lattice points (O), (B), (L) are considered to lie in the plane of incidence. In this case the three points lie in the constraint surface for rocking curves and for measurements made at constant incident direction, but varying energy.

It is possible to make semiquantitative predictions about the reflected intensities and total forward-diffracted wave fields based on the properties of the Bloch waves associated with certain special sets of points on the dispersion surface. In particular, it is of interest to determine which Bloch waves have one plane-wave component of zero amplitude and specifically to investigate when the dynamic interaction is such that in a multiple-beam approximation, one of the diffracted waves is extinguished.

(*i*) *Condition for Zero Amplitude of One Plane-Wave Component of the Bloch Wave*

In Eqs. (6) it is possible to arbitrarily specify the amplitude of one and only one plane-wave component ϕ_i. In the three-field case it is possible to examine the consequences of requiring one plane-wave component of the Bloch wave to be zero. If in the matrix equation describing the three-field interaction, one arbitrarily sets $\phi_0=0$, then

$$\begin{pmatrix} \delta_0 & U_B & U_L \\ U_{-B} & \delta_B & U_{L-B} \\ U_{-L} & U_{B-L} & \delta_L \end{pmatrix} \begin{pmatrix} 0 \\ \phi_B \\ \phi_L \end{pmatrix} = 0. \quad (20)$$

Therefore, the two conditions imposed on $(\mathbf{K}, E)$ and ϕ_0 and ϕ_i, in order that $\phi_0=0$, are

$$\begin{vmatrix} \delta_B & U_{L-B} \\ U_{B-L} & \delta_L \end{vmatrix} = 0, \quad (21a)$$

and

$$U_B\phi_B + U_L\phi_L = 0. \quad (21b)$$

The equation of the dispersion surface can be written as

$$F_{OBL}(\mathbf{K}, E) = 0 = \delta_0 \begin{vmatrix} \delta_B & U_{L-B} \\ U_{B-L} & \delta_L \end{vmatrix} - U_B \begin{vmatrix} U_{-B} & U_{L-B} \\ U_{-L} & \delta_L \end{vmatrix} + U_2 \begin{vmatrix} U_{-B} & \delta_B \\ U_{-L} & U_{B-L} \end{vmatrix}. \quad (22)$$

The first of Conditions (21) is identical to the equation of the dispersion surface in the two-beam (K_B, K_L) approximation. Since Eqs. (21) and (22) must be simultaneously satisfied, it is seen that $\phi_0=0$ is associated with those points on the three-beam dispersion surface $F_{OBL}(\mathbf{K}, E)=0$ along the line of intersection with the two-beam dispersion surface $F_{BL}=0$. This line, defined by

$$-U_B \begin{vmatrix} U_{-B} & U_{L-B} \\ U_{-L} & \delta_L \end{vmatrix} + U_L \begin{vmatrix} U_{-B} & \delta_B \\ U_{-L} & U_{B-L} \end{vmatrix} = 0 \quad (23)$$

for crystals with a center of symmetry, is

$$\delta_B = \mathbf{K}_B^2 - \mathbf{K}^2 = U_B U_{L-B}/U_L,$$
$$\delta_L = \mathbf{K}_L^2 - \mathbf{K}^2 = U_{B-L} U_L/U_B. \quad (24)$$

Furthermore, this line always lies on the plane*

$$2\mathbf{K}_B\cdot(\mathbf{L}-\mathbf{B}) = -(L-B)^2 + (U_{B-L}U_L/U_B) - (U_B U_{L-B}/U_L), \quad (25)$$

independent of energy.†

Similar conditions exist in order that ϕ_B or ϕ_L be zero. The Bloch waves $(\phi_0, 0, \phi_L)$ and $(\phi_0, \phi_B, 0)$ map onto the intersections of $F_{OL}(\mathbf{K}, E)=0$ and $F_{OB}(\mathbf{K}, E)=0$ with $F_{OBL}(\mathbf{K}, E)=0$, respectively. These intersections lie on the planes

$$\phi_B=0: \quad 2\mathbf{K}_0\cdot\mathbf{L} = (U_{-L}U_{L-B}/U_{-B}) - (U_L U_{-B}/U_{L-B}) - L^2, \quad (26a)$$

$$\phi_L=0: \quad 2\mathbf{K}_0\cdot\mathbf{B} = (U_B U_{B-L}/U_{-L}) - (U_B U_{-L}/U_{B-L}) - B^2. \quad (26b)$$

(*ii*) *The Mixed Bragg-Laue Case*

Figure 8 shows the dispersion surface for the three-beam symmetrical case, where B lies on the Brillouin zone boundary associated with L. The equations of "zero" planes in this case, where $U_{B-L}=U_B$, reduce to

$$\phi_0=0: \quad 2\mathbf{K}_B\cdot(\mathbf{B}-\mathbf{L}) = -(L-B)^2 + [U_L - (U_B^2/U_L)]; \quad (27a)$$

$$\phi_B=0: \quad 2\mathbf{K}_0\cdot\mathbf{L} = -L^2; \quad (27b)$$

$$\phi_L=0: \quad 2\mathbf{K}_0\cdot\mathbf{B} = -B^2 + [(U_B^2/U_L) - U_L]. \quad (27c)$$

The trace of these planes in the plane of the figure is shown, and the positions of the points associated with zeros in the Bloch waves are indicated in Fig. 8(d). It must be noted that, although the planes of the intersections exist independent of energy, the zeros in the Bloch waves exist when and only when the three-beam and two-beam dispersion surfaces intersect at the values given by Eq. (24), which may possibly occur only at complex values of $\mathbf{K}_0$; thus the zeros do not necessarily appear on the dispersion surface in real $\mathbf{K}$ space.

---

* For crystals without a center of symmetry these are two lines, one given by Eq. (24), the other by $\delta_B = U_{-B}U_{B-L}/U_{-L}$ and $\delta_L = U_{L-B}U_{-L}/U_{-B}$.

† $\mathbf{K}_L = \mathbf{K}_B + (\mathbf{L}-\mathbf{B})$; $\mathbf{K}_L^2 = \mathbf{K}_B^2 + (\mathbf{L}-\mathbf{B})^2 + 2\mathbf{K}_B\cdot(\mathbf{L}-\mathbf{B})$, $\mathbf{K}_L^2 - \mathbf{K}^2 = (\mathbf{K}_B^2 - \mathbf{K}^2) + 2\mathbf{K}_B\cdot(\mathbf{L}-\mathbf{B}) + (\mathbf{L}-\mathbf{B})^2 = U_{B-L}U_L/U_B$.

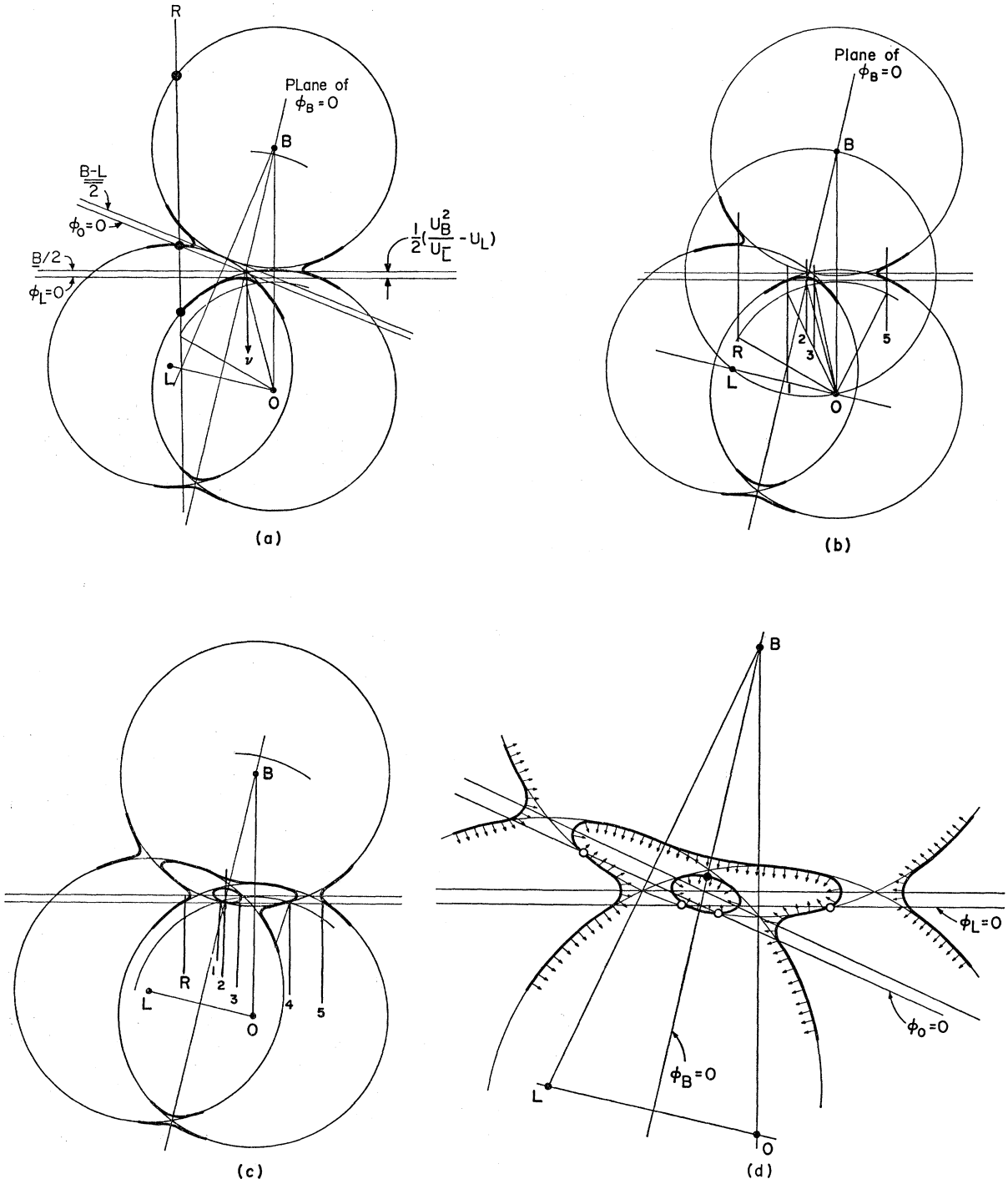

FIG. 8. Three-beam dispersion surface for the symmetrical case where the Bragg reflection **B** lies in the Brillouin zone boundary of the Laue reflection **L**. For the Bragg reflection to appear in the specularly reflected beam, the crystal normal ν must be parallel to **OB**. The dispersion surface is shown for an energy below the symmetry point [Fig. 8(a)]; at the symmetry point [Fig. 8(b)]; and above the symmetry point [Fig. 8(c)]. The position of the Ewald sphere is shown near the reciprocal lattice point **B**. It passes through the origin and the reciprocal lattice point **L** in the three cases. During a rocking curve the crystal normal moves from the orientation of R to 5. The planes in which the crystal plane wave associated with the reflections **B**, O, and **L** are identically zero are shown ($\phi_B = 0$, $\phi_L = 0$, $\phi_O = 0$). An enlarged diagram of the region of dispersion is shown in 8(d): the direction of the energy flow is indicated as is the allowed point (ϕ_i, ϕ_j, 0) (filled circle) and the unallowable points (open circles).

The ratios of the nonzero components of the wave fields are given by the condition (21b):

$$\phi_0=0: \quad \phi_B/\phi_L=-U_L/U_B;$$
$$\phi_B=0: \quad \phi_L/\phi_0=-1;$$
$$\phi_L=0: \quad \phi_B/\phi_0=-U_B/U_L. \tag{28}$$

Thus, in the symmetric case the position of the Bloch waves of $\phi_B=0$ are of particular interest for two reasons:

(a) At this angle one expects a minimum in the reflected Bragg intensity.

(b) Since $\phi_L/\phi_0=-1$, this is exactly the condition for the anomalous penetration or Borrmann effect in the forward-diffracted beam. In LEED, anomalous penetration is associated with reduced secondary emission which is then simultaneously observable with the Bragg minimum.

In general, in an Nth-order approximation $\phi_{G_i}=0$ for those Bloch waves which map onto the intersection of the surfaces $F_{0\ldots G_i\ldots G_{N-1}}(\mathbf{K}, E)=0$ and $F_{0\ldots G_{i-1},G_{i+1}\ldots G_{N-1}}(\mathbf{K}, E)=0$.

A detailed discussion of the application of these concepts to experimental observation follows.

D. Behavior of the Plane-Wave Amplitudes During an Experiment

Figure 8 shows the dispersion surface for the symmetrical three-beam case where the Bragg reflection lies on the Brillouin zone boundary of the Laue reflection. For the Bragg reflection to appear in the specularly reflected beam, the surface normal must be parallel to **B**. The three diagrams show the dispersion surface at energies (a) just below the symmetrical case, (b) at the symmetrical case, and (c) above the symmetrical case.

From Eq. (26) it can be seen that it is possible to draw the intersection of the surface in which one plane-wave component will be zero with the plane of the drawing as a straight line, parallel to the Brillouin zone boundary, but displaced by an amount given by Eq. (27). The planes for which $\phi_L=0$, $\phi_B=0$, and $\phi_0=0$ are shown as are the Brillouin zone boundaries: The plane for $\phi_B=0$ is identical to the Brillouin zone boundary of the Laue reflection L, in this case.

In Fig. 8(a), the surface normal ν is shown for a particular angle of incidence. At the energy of Fig. 8(b), this angle of incidence excites the symmetric three-beam case exactly, and the Ewald sphere passes through the reciprocal lattice points 0, L, and B. The Ewald sphere is shown in its entirety in Fig. 8(b), and arcs of the Ewald sphere for the same incident direction are shown near to the reciprocal lattice point B in Figs. 8(a) and 8(c). The reflection L is excited almost equally for the three energies at this orientation because it lies near the origin. The behavior of the crystalline plane waves during a true rocking curve can be discussed in terms of the intersection of the surface normal with the dispersion surface as the former is swept across the diagram. The positions of the surface normal corresponding to particular orientations of the incident beam are labeled on the diagrams.

For an arbitrary orientation of the incident beam, the surface normal will make, at most, $2N$ intersections with the real dispersion surface; in this case $2N\leq 6$.* Since only those Bloch waves which correspond to allowed directions of electron transport have a physical meaning, in a semiinfinite crystal there will only be N tie points excited.

In Fig. 8(a), for the orientation of the incident beam R, the surface normal is seen to have six intersections with the dispersion surface. The three physically excitable tie points are indicated by closed circles.

In Fig. 8(a), for the orientation of the incident beam ν, there is only one real tie point excited near the region of large dispersion: The Bloch wave at this point contains three strong plane-wave components. For an orientation slightly counterclockwise from this position, the Bloch wave is described by $(\phi_0, 0, \phi_L)$. A rocking curve at this energy about the orientation ν would show a specularly reflected beam having a strong minimum in the intensity at that orientation for which $\phi_B=0$. Over this same range of orientations, the Bragg reflection is excited since the surface normal passes through the gap in the dispersion surface: Any attempt to calculate the reflected intensity must take into consideration the evanescent waves associated with the gap. It should be noted that the presence of the third reflection (L) results in an increase in width of the gap over and above that width expected for the two-beam case of the Bragg reflection alone. This effect can be seen in Fig. 8(b), where the Bragg reflection occurs for the range of orientation R–5 in the three-beam case: The two-beam Bragg gap would occur for the range 1–5. Except for the zeros predicted by Eq. (27), three strong plane-wave components are excited near the appropriate two-beam intersections (Laue points) in each case, the third reflection notwithstanding.

For the energy of Fig. 8(c), it can be seen that during a rocking curve, the surface normal passes through a sequence of two-beam intersections: a Bragg reflection in the region R–1, a Laue reflection in the region 1–3, and a second Bragg region 4–5. The position of the tie points corresponding to the excitation of Bloch waves with only two nonzero plane-

* The remaining solutions correspond to those "gap" evanescent waves which must be included in the $2N$ solutions.

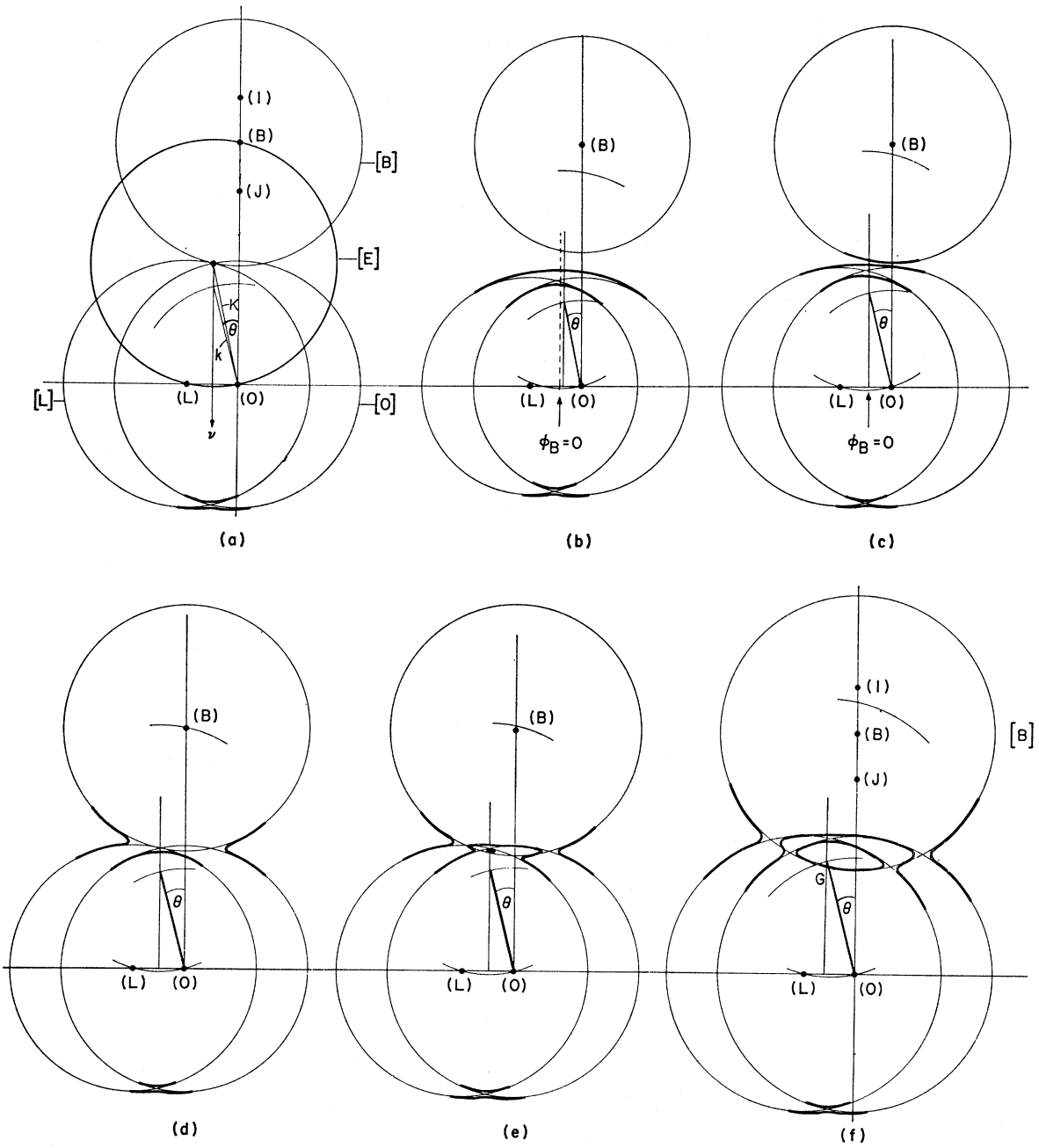

FIG. 9. (a) Construction for the Ewald sphere $[E]$ at an incident direction θ for a vacuum wave vector $\mathbf{k}$, crystal wave vector $\mathbf{K}$. The free-electron constant-energy spheres $[0]$, $[B]$, $[L]$ are drawn about the three reciprocal lattice points, 0, B, L, respectively. (b)–(f) The constant-energy dispersion surface (NFEA, heavy curve; free-electron approximation, light circles) for energies from below to above the excitation of the symmetrical three-beam case. The incident direction is maintained constant in the figure showing the behavior of the crystal normal during a typical intensity-vs-voltage (pseudorocking) curve.

wave amplitudes are shown in Fig. 8(d), which is an enlarged drawing of the region of the dispersion of Fig. 8(c). The direction of the energy flow is shown for each sheet of the dispersion surface. The intersections for each plane $\phi_L=0$, $\phi_B=0$, $\phi_0=0$ are shown at the appropriate sheet of the dispersion surface: The intersection on an excited sheet is indicated by a filled circle, on an unexcited sheet by an open circle.*

* The condition for $\phi_B{}^j=0$ occurs on the low-absorption sheet (j) of the dispersion surface. The accompanying excitation of the high-absorption sheet (i) is at the point of maximum absorption (the diameter point) so that the plane wave $\phi_B{}^i$ will have a negligible contribution to the amplitude of the crystalline Ewald wave field ψ_B.

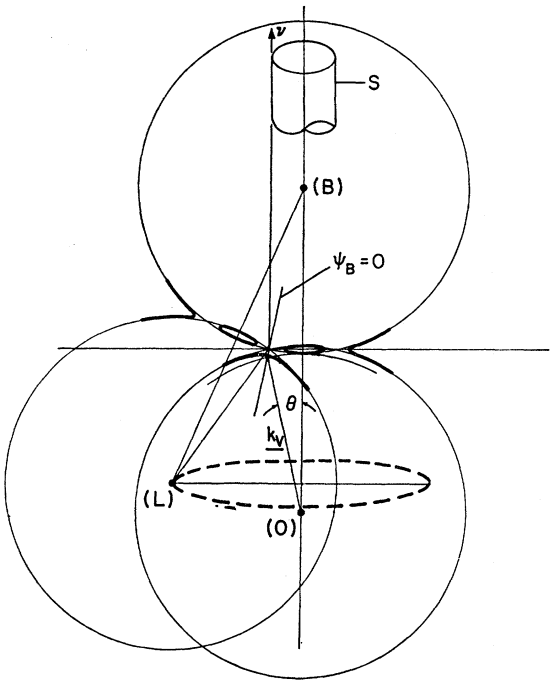

FIG. 10. Schematic drawing of the dispersion surface during a rotation diagram. During the rotation the magnitude of the incident wave vector **k** and the diffraction angle θ (measured from the crystal normal) remain constant, and the plane of incidence containing the origin and the incident wave vector is rotated about the surface normal. The cylindrical constraint surface (S) generated by the surface normal ν during the rotation is shown at the top of the figure. A reflection **L** is shown which corresponds to the excitation of the symmetrical three-beam case of Fig. 9.

Due to the conservation of current, as the surface normal excites successive tie points during a rocking curve, the intensity associated with a particular reflection changes continuously as the relative plane-wave amplitudes change. The intensity of the Bragg reflections observed in low-energy electron diffraction will exhibit fine structure which on purely kinematical arguments would appear to be anomalous.

A unique prediction of this N-beam model is the existence of geometries for which the Bragg reflected intensity exhibits a minimum (equal to zero if the contribution of the evanescent waves to the surface matching is ignored). A detailed discussion of the experimental observation of such minima in the three-beam mixed Bragg–Laue case will be published elsewhere.

Figure 9 shows a drawing of the three-beam dispersion surface [Eq. (18)] for several energies. The Ewald construction is shown in Fig. 9(a) for the simultaneous excitation of the points $(0)(L)(B)$. If the surface normal (ν) is chosen as shown, then B becomes a Bragg reflection and L becomes a Laue reflection. The circular free-electron constant-energy surfaces are also drawn. Figure 9(b) is drawn for an energy which excites only the Laue reflection strongly. The Ewald sphere is always far from the reciprocal lattice point B, and the Bragg reflected intensity (in the specularly reflected beam) is a minimum for the orientation shown. At this energy the presence of the dispersion sheet $F_B(\mathbf{K}, E)=0$ does not effect the dispersion sheets $F_{OL}(\mathbf{K}, E)=0$, which appear as for the two-beam case. As the energy is increased while the incident direction is maintained constant [9(b) through 9(f)], the dispersion in sheet $F_B(\mathbf{K}, E)=0$ increases as the Bragg reflection is excited; a gap finally develops in the constant-energy surface furthest from the origin. At still higher energies the gap moves off as a new dispersion sheet appears, and the Bragg reflection is no longer strongly excited as the same incident direction. It should be noted that the geometries of Figs. 9(b) and 9(f) are identical, an indication of the fact that, in general, the many weak Bragg reflections need to be considered only as a perturbation to the two-beam Laue case.

The difficulty in describing the behavior of the intensity measured during a pseudorocking curve where the energy is varied, but the incident beam direction is maintained can be seen from the sequence of Fig. 9. For each energy the dispersion surface must be constructed and the relative plane-wave amplitude calculated. In addition, the contribution of the evanescent waves in the gaps must also be taken into account. As the energy is varied, not only do various sheets of the dispersion surface appear in the region of the surface normal, but the positions of the zeros determined by Eq. (27) are also swept past the individual tie points, as is the case in Figs. 9(b)–9(d). In particular, for the diffraction geometry of Fig. 9(c), the wave field propagating in the direction of the Bragg reflection is essentially zero, since the tie point on the sheet of constant-energy dispersion surface enclosing (B) is unexcited, the tie point on the middle sheet of the dispersion surface excites plane waves which are strongly absorbed, and the tie point nearest O, L has an exact zero in the Ewald field Ψ_B. For this geometry, the surface matching would predict a zero in the intensity of the specularly reflected beam. This zero appears on the low-energy shoulder of the Bragg reflection which has a maximum at the energy of Fig. 9(d).

The behavior of the reflected intensity during a rotation diagram can be determined from inspection of Fig. 10. If the incident direction and energy are chosen such that the Bragg reflection B is excited, then for the surface normal parallel to **K**, a maximum in the specular intensity is observed. If multiple diffraction is ignored ($U_H=0$, $\mathbf{H}\neq\mathbf{B}$), then during the rotation, the cylindrical constraint surface (S) swept out by the surface normal (shown at the top of the figure) does not intersect a sheet of the dispersion hypersurface. In this case, no crystalline plane wave is excited and the incident plane wave is totally reflected with constant amplitude for all orientations of the plane of incidence. The magnitude of the

evanescent wave in the gap is invariant during the rotation. If multiple diffraction is introduced, then a number of reflections will be excited during the rotation. For a particular reflection L, there will be some orientation of the plane of incidence containing the three reciprocal lattice points 0, L, B. This corresponds to the geometry discussed in the previous sections. In general, near this orientation, a sheet of the dispersion hypersurface associated with an arbitrary reflection L will be excited, giving rise to a crystalline plane wave resulting in a decrease in the amplitude of the specularly reflected beam (conservation of current). For the symmetrical geometry shown in Fig. 10, the amplitude of the crystalline Ewald reflection Ψ_B will be zero for the orientation shown. This will be true for the case of any reciprocal lattice point lying on the circle passing through **L**. Rotation diagrams should therefore be characterized by minima in the specularly reflected intensity associated with the excitation of simultaneous reflection (Gervais, Stern, and Menes, 1968; Stern, Taub, and Gervais, 1969; Stern, 1968).

E. Relative Amplitude of Crystalline Reflections

A calculation of the amplitude of the various crystalline reflections in terms of the magnitude of the Fourier coefficients of the crystal potential for particular crystals (Vainsthein, 1964) is beyond the scope of this discussion. It is, however, appropriate to discuss qualitatively the relative amplitudes of the crystalline plane waves in order to give some insight into the degree of approximation made in considering a particular two- or three-beam case.

In a real crystal at finite temperature the effect of the thermal motion of the atoms is to reduce the strength of a reflection **H** by a term which can, to a first approximation, be written as $\exp(-M_H)$. This term, known as the Debye–Waller factor (James, 1965) should be associated with each of the Fourier coefficients of Eq. (6). At constant temperature, M_H is proportional to $H^2=h^2+k^2+l^2 \propto \sin^2\theta/\lambda^2$. Therefore, the plane waves in the two-beam approximation have amplitudes proportional to $U_H \exp(-M_H)$, and have the greatest magnitude for the smallest values of $\mathbf{H}^2$.

For the case of nongrazing incidence on low-index single-crystalline planes, these low-index reflections are of the Laue type. For typical crystals at moderate energies (100–1000 eV), Bragg reflections have relative amplitudes of about one order of magnitude smaller than Laue reflections. In the mixed Bragg–Laue case discussed above, the Bragg reflection can be expected to be very weak compared to the Laue reflection. If for one orientation of the incident beam a low-index Laue reflection lies on the sphere of reflection, many Bragg reflections will be excited as the incident direction is varied in a rocking curve, before a different strong Laue reflection is excited. Since these Bragg reflections of large **H** will in general be weak, they can be considered as a perturbation on the two-beam case. In LEED, only reflected (Bragg) intensities can be measured directly. The forward-scattered (Laue) wave field can only be determined indirectly in terms of such processes as the secondary emission. The two-beam approximation can therefore be considered appropriate in many cases over a large range of magnitudes of the dynamic diffraction variables when the effects observed depend primarily on the forward-scattered wave field. The three-beam case will be a valid approximation when the particular single Bragg reflection being observed is excited along with a low-index Laue reflection. A discussion of LEED experiments in terms of the two- and three-beam approximation will be published elsewhere.

F. Inclusion of Inelastic Processes

The discussion of the fundamentals of band theory and diffraction theory has been presented in terms of elastic processes which conserve both total energy and phase. In the discussion of diffraction effects in real crystals, the concept of absorption has been introduced in a phenomenological manner which disregards the nature of the inelastic processes themselves, but which allows the inclusion of additional selection rules and predictions resulting from the existence of such processes.

The net absorption of the total crystalline wave field is dependent on the details of the diffraction geometry. Although the forward-scattered wave field is inaccessible to direct measurement in low-energy electron diffraction, it can be investigated by measuring the secondary emission which is directly sensitive to the details of the net absorption. Since electrons inelastically scattered deep in the crystal under conditions of low net absorption have a small probability of reaching the surface, they do not contribute to the secondary current (Taub and Stern, 1968; Stern and Taub, 1968).

There are several important types of inelastic-scattering mechanisms which must be considered: those which result in significant energy losses and incoherence (Lax, 1957) of the scattered electrons (atomic excitation and plasma, or conduction electron, excitation) (Pines, 1964; Yoshioka, 1957; Lax, 1957; Honjo and Mihama, 1954; Kamiya and Uyeda, 1961; Hashimoto, Howie, and Whelan, 1962; Meyer, 1967; Goodman and Lehmpfuhle, 1967; Whelan, 1965; Radi, 1968; Borrman, 1941) and those which are essentially quasielastic and coherent (phonon excitation). The latter have been discussed previously by two of the authors (R. S. and J. P.) (Aldag and Stern, 1965) and others (McKinney, Jones, and Webb, 1967; Takagi, 1958; Yoshioka and Kainuma, 1961; 1962; Hall and Hirsch, 1965).

Neglecting the possibility of anisotropy in the ex-

citation of conduction electrons (Pines, 1964), the principle source of absorption in the crystal dependent on the details of the wave field is the possibility of atomic excitations: The transition probability for such excitations is proportional to the wave amplitude and to the local density of bound electrons. In the two-beam Laue case, the plane waves propagating from each of the two sheets of the dispersion surface are out of phase with each other: At the diameter points the wave associated with the dispersion surface nearest to the origin has nodal planes parallel to and situated at the atomic planes of the reflection; the wave associated with the dispersion sheet farthest from the origin has antinodes on these same planes. The latter wave therefore suffers anomalous absorption, while the former wave is anomalously transmitted. Far from the diameter points, all waves propagate with the same absorption coefficient.

It is possible to develop the Bethe theory in a periodic solid where absorption is included by writing Eq. (4) with an additional term in order to phenomenologically include all inelastic processes (Yoshioka, 1957):

$$(\mathbf{K}_G^2-E_K)\phi_G+\sum_H U_{H-G}\phi_H+\sum_H C_{HG}\phi_H=0, \quad (29)$$

where the coefficients of the additional term are complex:

$$C_{HG}=C_{HG}{}^r+iC_{HG}{}^i. \quad (30)$$

The general development of the theory of inelastic scattering (Lax, 1957; Honjo and Mihama, 1954; Kamiya and Uyeda, 1961; Hashimoto, Howie, and Whelan, 1962; Meyer, 1967; Goodman and Lehmpfuhle, 1967; Whelan, 1965; Radi, 1968), and in particular that based on Eq. (29), contains predictions of all the diffraction effects arising from the existence of inelastic processes including the Borrmann effect (Borrmann, 1941), secondary emission, and Kikuchi lines. In addition, the anisotropy of the Auger spectra based on the details of the allowed atomic excited states can also be predicted.

If in Eq. (30), $C_{OH}{}^i=U_H'$, and $C_{00}{}^i=U_0'$, then the absorption can be thought of as being associated with the complex Fourier coefficients of the crystal potential:

$$U_G=U_G''+iU_G'. \quad (31)$$

This treatment is not as general as that allowed by Eq. (29), since it does not include the details of the crystalline excited states.

The primary effect of the inclusion of absorption on the discussion of the elastic diffraction is a decrease in the intensity and asymmetry in the shape of the observed reflections, compared to the elastic case. Furthermore, the coefficients of each of the plane waves in Eq. (16) now acquire the form

$$C_i=c_i\exp(-\mathfrak{y}\cdot\mathbf{r}),$$

where $\mathfrak{y}$ is the vector absorption coefficient determined by the solution of Eq. (29), independent of the complex nature of $\mathbf{K}$; i.e., plane waves of real $\mathbf{K}$ are attenuated.

G. Summary

The electronic band and dynamical diffraction theories are different but essentially equivalent methods of treating the propagation of electron waves in periodic solids. In this paper there is developed a unified approach to the problem in terms of a seven-dimensional hypersurface in energy-complex $\mathbf{K}$ space, the dispersion hypersurface, which defines the totality of allowed solutions for an electron in a periodic crystal. The usual energy band diagram of band theory is the constant $\theta, \varphi, \mathbf{K}_i=0$ section of this surface. The dispersion surface of dynamical diffraction theory is a section at constant $E, \mathbf{K}_i=0$.

The dispersion hypersurface is a general property of the crystal. Discussion of any diffraction problem requires careful application of the constraints introduced by the boundary conditions of a particular experiment in order to select, from the entire set, those wave functions excited in that experiment. For an idealized crystalline surface these conditions immediately reduce the dimensionality of the hypersurface in imaginary $\mathbf{K}$ space. Conservation of total energy and momentum determines a geometrical constraint surface, the intersection of which with the dispersion hypersurface fixes the subset of all allowed wave functions that can be excited. For a semi-infinite crystal, the requirement of finite electron densities everywhere selects, from this subset, only those eigenfunctions which carry current into the crystal. Application of the continuity condition at the surface then determines the relative amplitudes of the several excited eigenfunctions.

The geometrical constraints imposed in real $\mathbf{K}-E$ space in the common diffraction experiments are examined. In particular the two classes of variable-energy experiment (pseudorocking curves) and the two classes of constant-energy experiment (rocking curves and rotation diagrams) are discussed in detail. In pseudorocking-curve experiments in which the direction of incidence is held constant, the most common experimental situation, it is necessary—in order to compare the data with theory—to calculate in detail a large sectional surface of the dispersion hypersurface; in pseudorocking-curve experiments in which $K_{||}$ is maintained constant, an experimentally difficult configuration, it is necessary only to calculate a (one-dimensional) curve on the dispersion hypersurface. The constant-energy experiments, i.e., those utilizing well-known x-ray techniques, are in principal straightforward and also require calculation only of a curve on the hypersurface.

The possibility of comparison of the results of a

given experiment with those of other experiments and with theoretical predictions depends critically on precise knowledge of the diffraction parameters. The low-index Laue reflections are very important in the generation of much of the complex fine structure observed in LEED. The two- and three-beam cases are developed in some detail as an illustration of some of the simple predictions of the theory. In the mixed Bragg–Laue three-beam case, zeros appear in the reflected Bragg intensities for certain geometries; the details of the experimental observations to be expected due to these zeros are discussed. The problem of inelastic scattering is mentioned briefly.

Although the present approach is appropriate at both low and high energies, there is no mention of the contribution of the crystal surface to the electron-diffraction intensities in the model used, since the periodicity of the semi-infinite crystal is maintained to the crystal–vacuum interface.

The main object of this paper has been the demonstration, primarily for heuristic reasons, of the essential unity underlying quite different approaches to the theory of electron diffraction. The present formulation is in fact an expansion of Bethe's N-beam theory, which is complete in that it has always allowed the possibility of inclusion of the complex $\mathbf{K}$ evanesant waves.

H. Conclusions

In order to understand LEED experiments it is necessary to consider the details of the dispersion hypersurface. The contribution of the near degeneracy close to, but not at, the points of high symmetry in the reciprocal lattice can best be demonstrated in this manner. The detailed contribution to LEED of the bulk band structure must be understood before the problem of the surface contribution to diffraction can be solved. A survey of the general problem shows that the strong reflections are in general those Laue reflections having low index. In the case of LEED measurements in back reflection, the important geometrical situation is that of the excitation of the mixed Bragg–Laue three-beam case. The constant-energy dispersion surface is shown to be particularly appropriate in determining the relative amplitudes of the crystalline plane waves excited in certain experiments. It is these constant-energy experiments which allow the most direct identification of the band structure responsible for the variation of the diffracted intensity as a function of the diffraction parameters.

In future both real and computer experiments should be done at constant energy in order to systematically explore the dispersion hypersurface and to determine the effects of the complex symmetries expected to influence LEED. Examination of the diffraction geometry for any real experiment shows that at energies where the first Born approximation (or any other currently used approximation) is valid, no simple ($N<10$) multiple-diffraction theory is really a justifiable approximation. In order to investigate the nature of the dispersion surface and the effect of weak reflections, inelastic and quasielastic scatterings, it will be necessary to perform measurements with precision comparable to that usually employed in x-ray diffraction. This sort of care has not been taken in LEED measurements in the past. The reflected intensities are extremely sensitive to the number and symmetries of the simultaneous reflections; this sensitivity is clearly illustrated by the Bragg–Laue case discussed in Sec. V. C. It would appear that an entire new generation of experiments is necessary—on atomically flat surfaces, at very low energies, with high angular precision—in order to explore properly and systematically the origins of the diffraction mechanisms, and to distinguish between the utility of the many LEED theories currently being developed.

ACKNOWLEDGMENTS

The authors wish to acknowledge helpful discussions with Professor H. Wagenfeld and Mr. H. Taub.

APPENDIX: DIRECTION OF ELECTRON CURRENT

Proof of the direction of electron current (Schrödinger flux):

$$\langle \mathbf{v} \rangle = \langle \mathbf{k} \mid (\hbar/im)\nabla \mid \mathbf{k} \rangle, \tag{A1}$$

where

$$\mid \mathbf{k} \rangle = \sum_G \phi_G \mid \mathbf{k}_G \rangle;$$

therefore

$$\langle \mathbf{v} \rangle = (\hbar/m) \sum_G \mid \phi_G \mid^2 \mathbf{k}_G. \tag{A2}$$

On the other hand, if one starts from the Schrödinger equation

$$[(\hbar^2/2m)\mathbf{k}_G^2 - E(\mathbf{k})]\phi_G + \sum_H V_{H-G}\phi_H = 0 \tag{A3}$$

and operates with ∇_k, one obtains

$$(\hbar^2/m)\mathbf{k}_G\phi_G - \nabla_k E(\mathbf{k})\phi_G = 0.$$

Multiplication by ϕ_G^* and summation over G yields

$$\sum_G (\hbar^2/m)\mathbf{k}_G \mid \phi_G \mid^2 - \nabla_k E(\mathbf{k}) \sum_G \mid \phi_G \mid^2 = 0,$$

and

$$\sum_G (\hbar^2/m)\mathbf{k}_G \mid \phi_G \mid^2 = \nabla_k E(\mathbf{k}).$$

Therefore, from Eq. (A2),

$$\langle \mathbf{v} \rangle = (1/\hbar)\nabla_k E(\mathbf{k}). \tag{A4}$$

However, in the units of this paper ($\hbar^2/2m=1$) it is necessary to rewrite Eq. (A1) as

$$\langle \mathbf{v} \rangle = \langle \mathbf{k} \mid (2/m)^{1/2}(\nabla/i) \mid k \rangle,$$

whereby Eq. (A4) becomes

$$\langle \mathbf{v} \rangle = (2m)^{-1/2}\nabla_k E(\mathbf{k}).$$

REFERENCES

J. P. Aldag and R. M. Stern, Phys. Rev. Lttrs. **14,** 857 (1965).
B. Batterman and H. Cole, Rev. Mod. Phys. **36,** 681 (1964).
H. Bethe, Ann. Phys. **87,** 55 (1928).
E. I. Blount, Solid State Phy. **13,** 306 (1962).
G. Borrman, Physik. Z. **42,** 157 (1941).
D. S. Boudreaux and V. Heine, Surface Sci. **8,** 426 (1967).
V. F. Dvoryankin and A. Yu. Mityagin, Kristallografi **12,** 1112 (1967) [Sov. Phys.—Crystallogr. **12,** 982 (1968)].
P. P. Ewald, Ann. Physik **49,** 1 (1916).
P. P. Ewald and Y. Heno, Acta Cryst. **A24,** 5 (1968).
E. Fues, Ann. Physik **36,** 209 (1936).
E. Fues, Ann. Physik **43,** 538 (1943).
A. Gervais and R. M. Stern, Bull. Am. Phys. Soc. **13,** 592 (1968) [Surf. Sci. (to be published)].
A. Gervais, R. M. Stern, and M. Menes, Acta Cryst. **A24,** 191 (1968).
P. Goodman and G. Lehmpfuhle, Acta. Cryst. **22,** 14 (1967).
C. R. Hall and P. B. Hirsch, Proc. Roy. Soc. (London) **A286,** 158 (1965).
W. A. Harrison, *Pseudopotentials in the Theory of Metals* (W. A. Benjamin, New York, 1956).
H. Hashimoto, A. Howie, and M. J. Whelan, Proc. Roy. Soc. (London) **A269,** 80 (1962).
R. D. Heidenreich, Phys. Rev. **77,** 271 (1950).
V. Heine, Surf. Sci. **2,** 1 (1964).
V. Heine, *Low Temperature Physics*, J. G. Daunt *et al.*, Eds. (Plenum Press, New York, 1965).
Y. Heno and P. P. Ewald, Acta Cryst. **A24,** 16 (1968).
G. Honjo, and K. Mihama, J. Phys. Soc. Japan **9,** 184 (1954).
R. W. James, Solid State Phys. **15,** 55 (1963).
R. W. James, *The Optical Principals of the Diffraction of X-Rays* (G. Bell and Sons, Ltd., London, 1965).
K. Kambe, Z. Naturforsch. **22a,** 22 (1967).
Y. Kamiya, and R. Uyeda, J. Phys. Soc. Japan **16,** 1361 (1961).
C. Kittel, *Introduction to Solid State Physics* (John Wiley & Sons, Inc., New York, 1956), 2nd ed.
C. Kittel, *Quantum Theory of Solids* (John Wiley & Sons, Inc., New York, 1962).
W. Kohn, Phys. Rev. **115,** 809 (1957).
J. B. Krieger, Phys. Rev. **156,** 776 (1966).
R. de L. Kronig, and W. G. Penny, Proc. Roy. Soc. (London) **130,** 499 (1931).
M. Lax, Rev. Mod. Phys. **23,** 287 (1957).
G. Lehmpfuhl, and A. Reiszland, Z. Naturforsch. **23a,** 544 (1968).
P. M. Marcus, and D. W. Jepsen, Phys. Rev. Letters **20,** 925 (1968).
J. T. McKinney, E. R. Jones, and M. B. Webb, Phys. Rev. **160,** 523 (1967).
E. G. McRae, J. Chem. Phys. **45,** 258 (1966).
G. Meyer, Z. Naturforsch. **21a,** 14 (1967).
K. Moliere, and H. Niehrs, Z. Physik **137,** 445 (1954).
P. M. Morse, Phys. Rev. **35,** 1310 (1930).
H. Niehrs, Z. Physik **138,** 570 (1954a).
H. Niehrs, Z. Physik **139,** 88 (1954b).
R. Peierls, Z. Physik **53,** 255 (1929).
P. Penning, Philips Res. Rept. **23,** 12 (1968).
P. Penning and D. Polder, Philips Res. Rept. **23,** 1 (1968).
D. Pines, *Elementary Excitations In Solids* (W. A. Benjamin, Inc., New York, 1964).
J. S. Plaskett, Proc. Roy. Soc. (London) **A301,** 363 (1967).
G. Radi, Z. Physik **212,** 146 (1968).
A. Sommerfeld, and H. Bethe, *Handbuch der Physik*, S. Flügge, Ed. (Springer–Verlag, Berlin, 1933), Vol. 24.
E. A. Stern, Phys. Rev. **162,** 565 (1967).
R. M. Stern, Proc. Am. Cryst. Assn. **4,** 14 (1968).
R. M. Stern, and H. Taub, Phys. Rev. Letters **20,** 1340 (1968).
R. M. Stern, H. Taub, and A. Gervais, *Structure and Chemistry of Solid Surfaces*, G. Somorjai, Ed. (John Wiley & Sons, Inc., New York, 1969).
S. Takagi, J. Phys. Soc. Japan **13,** 278 (1958).
H. Taub, and R. M. Stern, Bull. Am. Phys. Soc. **13,** 592 (1968).
M. Tournarie, J. Phys. Soc. Japan Suppl. BII **17,** 925 (1962).
B. K. Vainsthein, *Structure Analysis by Electron Diffraction* (Pergamon Press, Inc., New York, 1964).
E. H. Wagner, Z. Naturforsch. **62,** 133 (1951).
M. J. Whelan, J. Appl. Phys. **36,** 2099, (1965).
H. Yoshioka, J. Phys. Soc. Japan **12,** 618 (1957).
H. Yoshioka, and Y. Kainuma, J. Phys. Soc. Japan Suppl. BII **17,** 134 (1962).